Towards MIGO, the *M*atter-wave *I*nterferometric *G*ravitational-wave *O*bservatory, and the Intersection of Quantum Mechanics with General Relativity

Raymond Y. Chiao and Achilles D. Speliotopoulos
University of California, Berkeley, CA 94720-7300

March 8, 2004

Abstract

A dynamical, non-Euclidean spacetime geometry in general relativity theory implies the possibility of gravitational radiation. Here we explore novel methods of detecting such radiation from astrophysical sources by means of matter-wave interferometers (MIGOs), using atomic beams emanating from supersonic atomic sources that are further cooled and collimated by means of optical molasses. While the sensitivities of such MIGOs compare favorably with LIGO and LISA, the sizes of MIGOs can be orders of magnitude smaller, and their bandwidths wider. Using a pedagogical approach, we place this problem into the broader context of problems at the intersection of quantum mechanics with general relativity.

1 Introduction

In this contribution to the proceedings of the 2003 Gargnano workshop on 'Mysteries, Puzzles, and Paradoxes of Quantum Mechanics', let us begin with a brief review of those basic notions of differential geometry that will be important for the understanding of the interaction between gravitational radiation and quantum matter. Specifically, we shall examine here matter-wave interferometry as a means of detecting gravitational radiation from astrophysical sources. In a pedagogical manner, we shall place this problem into the broader context of some of the fascinating problems at the intersection of quantum mechanics with general relativity.

One of Euclid's axioms for plane geometry is the *parallel-lines axiom*, i.e., that parallel lines never meet, no matter how far these lines are extended in either direction. This axiom is illustrated by figure 1(a). We shall presently extend this axiom of Euclidean geometry to a statement about worldlines of test particles in flat spacetimes in general relativity.

Gauss discovered *non-Euclidean* geometry after a deliberate omission of this Euclidean axiom [1, 2]. He found one example of this geometry in the surface of a sphere, where there exists a constant positive curvature everywhere. This Gaussian geometry is illustrated in figure 1(b). A violation of the Euclidean axiom can be illustrated by extending northward two initially parallel 'lines of longitude' starting at points O and P at the equator. These lines of longitude are *geodesics*, i.e., the 'straightest' possible lines between two points, which minimize the intervening distance between them. When these geodesics are extended north, they will converge onto, and eventually intersect at, the north pole N, thus violating Euclid's parallel-line axiom.

Riemann generalized Gauss's notion of non-Euclidean geometry to that of *differential geometry* for arbitrarily curved manifolds [2]. As a measure of local curvature, he introduced the operational method of the *parallel transport* of a vector around an infinitesimal circuit, i.e., a tiny closed curve on a differentiable manifold. After the parallel transport is completed, there results a rotation of the final direction of the parallel-transported vector by an angle ϕ with respect to its initial direction, as illustrated in part (b) of figure 1. This rotation angle ϕ is thus a measure of the local curvature of the manifold.

To quantify this angle ϕ, Riemann introduced his curvature tensor R^l_{ijk}, which we define following

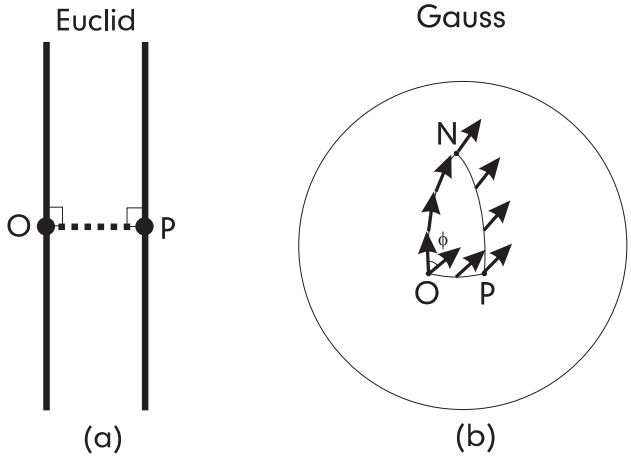

Figure 1: (a) Euclid's parallel-lines axiom in plane geometry states that two straight, parallel lines, such as the ones extended through the nearby points O and P, never meet at infinity. Gauss discovered a non-Euclidean geometry which is illustrated in (b). Two parallel geodesics on a sphere, represented by two lines of longitude emanating from points O and P on the equator of the sphere, converge onto the north pole N. Parallel transport of a vector around the spherical triangle ONP, and back to O again, illustrates the Gauss-Bonnet theorem, which states that the sum of the three interior angles of a triangle is 180° plus the solid angle subtended by this triangle with respect to the centre of the sphere. Here ϕ is the rotation angle of the parallel-transported vector after its completion of the circuit. In Berry's phase, an 'anholonomy' is the quantum phase factor $\exp(im_s\phi)$ that a spin with component m_s normal to the surface would pick up after adiabatic transport around the circuit OPNO in the field of a magnetic monopole located at the centre of the sphere.

Landau and Lifschitz's approach as [3]:

$$\delta\xi_i = -\frac{1}{2}R^l_{ijk}\delta f^{jk}\xi_l \tag{1}$$

where the Latin indices i, j, k, l, which run from 1 to 2 to 3, represent the three spatial dimensions, ξ_l are components of the initial vector, and $\delta\xi_i$ are the changes of the final vector components relative to the initial components, after the process of parallel transport of the vector around a closed circuit—with a infinitesimal area given by $\delta f^{jk} = \delta x^j \delta x^k$—is completed (Einstein's summation convention is used here for repeated indices).

Einstein generalized Riemann's notion of curved *space* to curved *spacetime* by the generalization of the curvature of space to that of the curvature of spacetime, so that

$$R^l_{ijk} \to R^\lambda_{\mu\nu\kappa} \tag{2}$$

where the Greek indices $\lambda, \mu, \nu, \kappa$ now run from 0 (representing time), to 1, 2, and 3 (representing space). He then applied the geometrical concepts of Gauss and Riemann to describe gravity: Matter acts on geometry by curving spacetime, and geometry acts on matter by determining the paths of test particles [4]. Flat spacetimes still obey Euclid's parallel-lines axiom, now generalized to the case of two straight and parallel *worldlines*, i.e., trajectories of noninteracting particles in space and time, for two small, nearby free objects at rest with respect to each other, e.g., in outer space, located, at time $t = 0$, in their proper frames at the two points O and P, as illustrated in figure 2(a). These two straight and parallel worldlines are also implied by the rectilinear, uniform motion of free objects obeying Newton's first law of motion.

In this space-time diagram, time, represent by the vertical axis, ascends vertically, and space is represented in one dimension by the horizontal axis. Thus one of the objects, say the observer O, is represented by a vertically ascending, straight worldline, and a nearby object P is represented by the nearby, parallel

worldline. If spacetime were strictly flat (as shown in figure 2(a)), these two straight and parallel worldlines would never meet. However, like the great circles on a sphere, or geodesics on a pseudosphere, in curved spacetimes these lines can either converge, or diverge from each other, respectively, depending on the sign of the components of the Riemann curvature tensor. An observer fixed on O would see the object P either come towards him, or go away from him, and would interpret this motion as being due to an effective 'tidal' force acting on P (see Chapter 1 of [4] for a description of this). In figure 2(b) we have drawn the specific case where components of the local Riemann curvature tensor are negative, and the worldlines diverge from one another. Since both the observer and the object are simply following their own worldlines—which are geodesics in the absence of all other forces on both the observer and the object—the equivalence principle still holds, and consequently this force is proportional to the mass of the object. The resulting motion of P as observed by O is therefore *independent* of the mass, composition, or thermodynamic state of the test object at P, and herein lies the *geometrical* meaning of the equivalence principle. Moreover, when the local Riemann curvature tensor between O and P can be approximated as a constant, this force, like the action of the Moon's gravity on the tides, *increases linearly* with the distance between O and P (see figure 2(b)), and indeed, the use of the name 'tidal' for this effective force comes from the tidal force on the oceans by the Moon's gravitational field.

It is important to note that while the worldline illustrations in figure 2 are a visualization of geometry, and its connection to gravity and gravitational tidal forces, they are only a convenience, and do not represent any frame that can be achieved physically. As drawn, the perspectives are that of an Observer who is removed from the spacetime, and standing outside of it looking in. This is unphysical. Every experimental measurement is made through an experimental apparatus—which may be as simple a device as a pair eyes used to see the motion of an object P a small distance away—that is, by necessity, a physical object. As such, the apparatus *must* lie along a worldline in the spacetime of the universe, and cannot be removed from it. *No* experimental measurements can be done by a fictitious observer 'suspended' outside of the universe.

Of particular interest to this paper is the case when a 'gravitational wave' (GW for short) is present in the spacetime. In this case the worldlines shown in figure 2(b) will periodically converge and diverge from each other, due to the fact that the curvature of spacetime is alternating between positive and negative values as the GW passes over the observer O and object P. Such distance changes between the two objects can be measured by sending a light beam out from O, and reflecting it by means of a mirror at P back to O. The distance between the two objects, measured in this way, will also change periodically in time when the GW passes over them. Once again the observer O would interpret the motion of the object P as due to an effective 'tidal' force which, in the limit of long-wavelength GWs, also grows linearly with the distance separating O and P (see Chapter 35 of [4] for a more detailed description).

Because of the experiment by Pound and Rebka [5] to measure the gravitational redshift, along with the experiment by Collela, Overhauser and Werner (COW) [6] to demonstrate through neutron interferometry that the gravitational potential of the Earth induces a quantum phase shift, the general relativistic effect most familiar to the Atomic, Molecular, and Optical (AMO) community is the gravitational redshift; GWs and their interaction with matter are not nearly as well known. There is thus an unfortunate tendency among the community to try to understand all general relativistic effects, including those due to GWs, in terms of the redshift. This cannot be done. If the redshift were used in an attempt to understand the physics of GWs, it would be like trying to understand electromagnetic (EM) waves using the scalar potential only; most of the essential physics would be lost.

Because of the AMO community's unfamiliarity, we present here a review of GWs. This review is necessarily brief; the literature on GWs, their generation, propagation and interaction with matter, is vast (see [4] and [7]), and a detailed presentation on the topic cannot be done within this paper. We will focus here on the physics that underlie GWs, and will delay the presentation of a mathematical review to **Appendix A**.

The existence of GWs is one of the most fundamental predictions of general relativity. Unlike the Newtonian gravitational potential, which can be obtained from general relativity by taking the appropriate non-relativistic and weak gravity limits, GWs do not have an analog in Newtonian gravity. This is because like electrostatics, Newtonian gravity is a static theory that cannot encompass wave propagation. Indeed, the analysis of the gravitational redshift, as measured in the Pound-Rebka experiment, could be done using only special relativity and the equivalence principle; it does not need the full structure of general relativity.

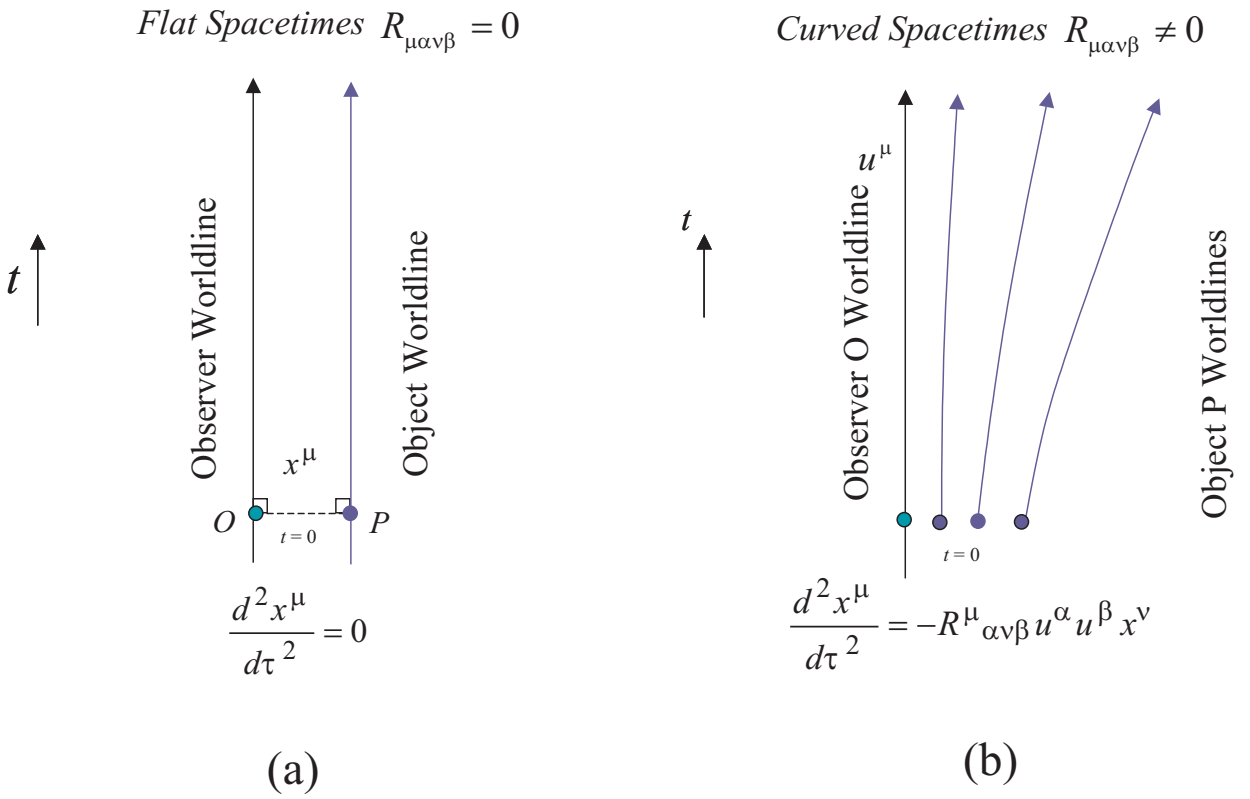

Figure 2: Euclid's parallel-line axiom applied to the flat spacetime shown in (a) implies that the worldlines of two small objects O and P at rest with respect to each other at $t = 0$, remain parallel to each other and never meet. In the curved spacetimes shown in (b), however, the two worldlines can either converge or diverge, or, as in the case of GWs, can oscillate. The acceleration of an object seen by the observer O close to P is proportional to the local Riemann curvature tensor, and is also proportional to the *separation* x^μ between O and P, as is the case in all such *tidal* effects.

Just as it took the discovery of Ampère's and Faraday's Laws to lead Maxwell to predict the existence of EM waves, it took Einstein's generalization of Newtonian gravity to predict the existence of GWs, and to describe their properties.

Many, but not all, of the underlying properties of GWs in the linear approximation can be understood [8] in analogy with EM waves (see **Appendix A**). Like EM waves, GWs have two physical polarizations—the + polarization and the × polarization—but unlike an EM wave, which is a spin 1 field and can be represented by a vector potential A_μ, a GW is instead a spin 2 field and must be represented by a second-rank *tensor* $h_{\mu\nu}$. This tensor is analogous to a local *strain* induced on spacetime by a GW, and is a measure of the size of the 'ripples' in spacetime caused by the passage of the GW. Like A_μ, $h_{\mu\nu}$ is 'gauge' field, with the choice gauge being a choice of *coordinate* systems, rather than a choice in a $U(1)$ phase factor. The gauge invariant object corresponding to the field strength $F_{\mu\nu}$ for EM is the Riemann curvature tensor $R^\lambda_{\mu\nu\kappa}$, constructed from second derivatives of $h_{\mu\nu}$. While it is possible to choose a gauge where $h_{00} \neq 0$—the term that would generate gravitational-redshift-like effects—this would not be the minimal gauge for the GW. Making this gauge choice would be analogous in EM to making a gauge choice where $A_0 \neq 0$ instead of the usual *radiation* gauge: $A_0 = 0$ and $\vec{\nabla} \cdot \vec{A} = 0$. Moreover, since the potential h_{00} can describe at most one of the two physical degrees of freedom of the GW, attempting to understand the effects of GWs on matter using this h_{00} through a gravitational redshift argument would miss much of the underlying physics. Both degrees of freedom for the GW must be taken into account, and this is most easily done by choosing a minimal

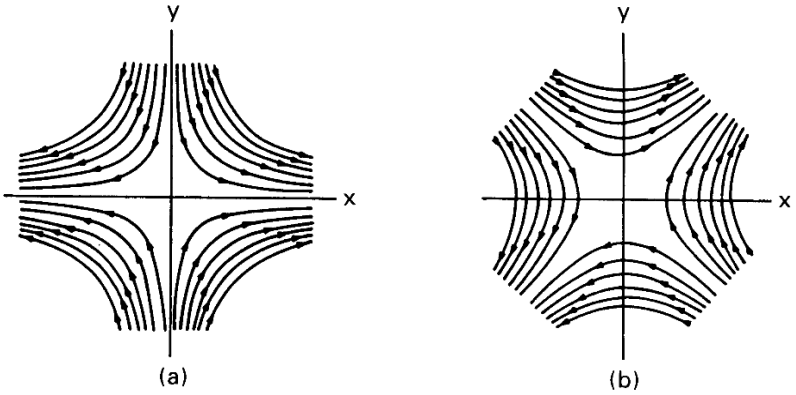

Figure 3: The force-field lines for the + polarization (a) and × polarization (b) of a GW (from [72]). These patterns are the snapshots of anisotropies of space, or 'strains', induced by the GW in the spacetime manifold, taken at $t = 0$ by an observer located at the centre, i.e., snapshots of the patterns of motion of an ensemble of freely-falling, noninteracting test particles distributed uniformly over the (x, y) plane. These time-varying patterns of anisotropies cause time-varying phase shifts to appear both for light waves in Michelson-type interferometers, such as in LIGO, and also for matter waves in Mach-Zehnder-type interferometers, such as in MIGO.

gauge. This gauge—which is analogous to the radiation gauge for EM waves—is the transverse-traceless (TT) gauge: $h^\mu_\mu = 0$, $\nabla^\mu h_{\mu\nu} = 0$, and for GWs propagating on flat ('Minkowski') spacetime, $h_{0\mu} = 0$. In particular, the gravitational potential vanishes since $h_{00} = 0$. There can be no gravitational-redshift-like effects; only the spatial 'strain' components h_{ij} are non-vanishing. Like A_μ, in this gauge h_{ij} can be represented as plane waves with two polarization vectors $\epsilon^{(+)}_{ij}$ and $\epsilon^{(\times)}_{ij}$, shown graphically on figure 3.

One aspect of GWs that *cannot* be understood in analogy with EM waves is the interaction of GWs with matter. The reason for this goes beyond the obvious differences in the tensorial ranks of $h_{\mu\nu}$ and A_μ. Unlike EM waves, GWs, like all gravitational effects, *cannot* be screened. As mentioned above, *all* physical observers must be part of spacetime, and cannot be removed from it. When a GW passes through a physical system, it acts on *all* parts of the system, including the observer, and consequently, only *differences* in the motion between the observer (O in figure 2) and the observed (P in figure 2) can be measured; the 'absolute' motion of either one cannot (see discussion in Chapter 35 of [4]).

If only *relative* motion can be measured when a GW is present, what coordinate system should be chosen? A description in words of this coordinate system has been given by Thorne [7], and has been outlined by Synge [10], and de Felice and Clark [11] for general spacetimes. More recently, Speliotopoulos and Chiao [12] has explicitly constructed this coordinate system for general spacetimes in the limit of linearized gravity. Its construction is based on the following physical constraints [13]: Every physical particle travels along a worldline in the spacetime of the universe. Every measurement of the physical properties of the test particle by an observer must be done using an experimental apparatus. Before the observer can take measurements with this apparatus, he must first choose a local orthonormal coordinate system. In curved spacetimes, this involves the construction of a *local* orthonormal coordinate system (a tetrad frame) [10]. Naturally,

this coordinate system will be fixed, say, to the centre of mass of his experimental apparatus, and will thus propagate in time along the worldline of the apparatus as well. The observer uses the coordinate time of the physical apparatus to measure time, which, because he or she will not be moving relative to the apparatus, is also his or her proper time. Thus the time axis of the coordinate system he or she has chosen will always be tangential to his or her own worldline. The position—which can be of finite extent—of the test particle is measured with respect to an origin fixed on the apparatus, and is the shortest distance between this origin and the particle. However, because the apparatus travels along its worldline, the origin of the coordinate system will also travel along a worldline in the spacetime. When the rate of change of the position of the particle is measured at two successive times, the *relative* four-velocity of the particle with respect to the apparatus will naturally be obtained (see [12] for this construction).

As described, it would seem that the observer simply constructs his or her usual laboratory frame, and it is difficult to see the novelty of this construction. The construction is done, however, in a *curved* spacetime, and as a result, in this coordinate system the observer O sees the object P in figure 2(b) undergoing an acceleration dependent upon the local Riemann curvature tensor of the spacetime. When no other forces are acting on the object, it is straightforward to show that when P is close to O, this acceleration is

$$\frac{d^2x_i}{dt^2} = -R_{0i0j}x^j = \frac{1}{2}\frac{d^2h_{ij}}{dt^2}x^j, \tag{3}$$

where R_{0i0j} are components of the Riemann curvature tensor. The second equality holds for the special case when long-wavelength GWs (see **Appendix A**)—which causes the deviations h_{ij} of the metric from flat spacetime—are present. This equation is obtained by taking the usual *geodesic* equation for the object P, subtracting from it the geodesic equation for the observer O, and expanding the result to first order in x^i, the distance separating O and P shown in figure 2(b). Equation (3) is the geodesic *deviation* equation of motion, and describes the *difference* in the motion between two nearby geodesics. Note that the acceleration in Eq. (3) is proportional to R_{0i0j}, *and is a gauge-invariant quantity*. Consequently, although the explicit dependence of this acceleration on h_{ij} depends on the choice of the TT gauge for the GW, the *dynamics* (or acceleration) of the object described by Eq. (3) will not, in the end, depend on this gauge (or coordinate) choice.

Turning now to geometry and quantum systems, Berry pointed out that non-Euclidean geometry can often be encountered in quantum mechanics [15] as well as classical mechanics. For example, a spin-half particle can be constrained by a strong magnetic field to always remain parallel to the direction of the field. When the direction of the magnet that produces this field is slowly rotated through space around a closed conical circuit, there results a rotation of the spin through the angle ϕ after the completion of a circuit. After this round trip, the spin picks up a quantum phase factor which is a consequence of the non-Euclidean geometry of the Bloch sphere (see figure 2(b)).

This phase factor can be explicitly seen through the Gauss-Bonnet theorem, which states that $\phi = \Omega$, where Ω is the solid angle subtended by the circuit with respect to the centre of sphere. There therefore results a quantum phase shift $\Delta\Phi$ experienced by the *rotated* spin after this round trip, where $\Delta\Phi = m_s\phi = m_s\Omega$ for the case where the spin stays adiabatically in its eigenstate $|m_s\rangle$. After the circuit is completed, the spin thus picks up a phase factor of $\exp(im_s\phi) = \exp(im_s\Omega)$ that can be measured in quantum interferometry. This is Berry's 'geometric phase factor', or 'anholonomy', which is similar to the Aharonov-Bohm phase factor picked up by an electron after it traverses a circuit on the surface of a sphere surrounding a Dirac monopole.

Irrespective of the great successes of differential geometric concepts in classical physics, since all objects at a fundamental level obey quantum mechanics, the notion of 'worldlines', or of 'geodesics', or of 'trajectories' in general, is problematic because of the uncertainty principle. As Bohr has taught us, we must fundamentally abandon the notion of *classical trajectories* in quantum mechanics. Nevertheless, from Berry's work it is well known that geometric concepts are fruitful in quantum mechanics as well. The crucial question then arises: How does one *operationally measure* spacetime curvature in a quantum world? As a corollary, how does one know whether a spacetime is *precisely* flat or not? The answer: By means of the interference of *quantum* test particles using matter-wave interferometry, as these test particles move through spacetime. These test particles are *quantum* in the sense that in the interferometer, we cannot know, even in principle, *which path*, in the quasi-classical limit, a given particle actually took. Hence we are strongly

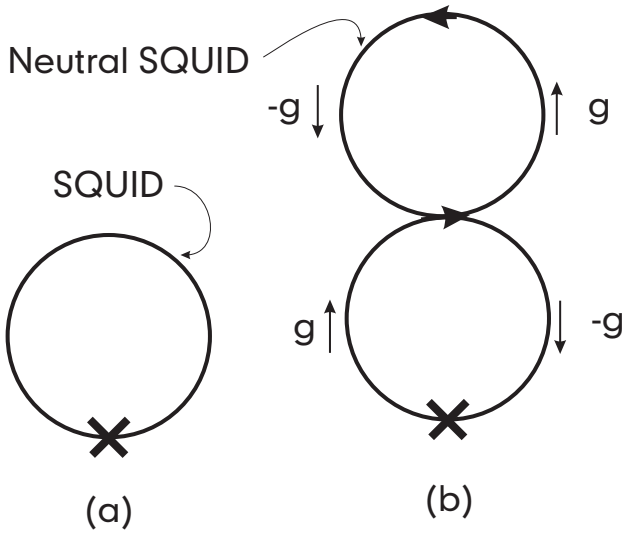

Figure 4: SQUIDs as detectors of long-range fields. 'X's denote Josephson junctions. (a) A superconducting SQUID is a sensitive detector of magnetic fields through the Aharonov-Bohm effect. (b) A neutral SQUID (e.g., using superfluid helium) could also in principle detect gravitational radiation through a gravitational version of the Aharonov-Bohm effect. As a GW with + polarization passes over the interferometer propagating from left to right, the left and right sides of the SQUID, which are spaced by half a wavelength of a GW, causes tidal forces that reverse in sign from left to right. These forces induce a time-varying phase shift, which can be detected by means of the Josephson junction.

motivated to examine the problem of matter-wave interference as a means of quantifying the problem of the *quantum measurement* of the curvature of time-varying spacetime geometries, and in particular, the specific case of those associated with gravitational radiation. This is closely related to the more general question: How does *gravitational* radiation interact with *quantum* matter? As we shall see below, this question already arises in an interesting way at the level of *nonrelativistic* quantum matter interacting with *weak, linearized* GWs. This problem is a *linear* one both in the matter and the field sectors of the theory, and should therefore be calculable using linear response theory.

One of the authors (RYC) started thinking about this problem two decades ago [16], when he asked the question: If the superconducting quantum interference device (SQUID), an early form of a matter-wave interferometer, can very sensitively measure the Aharonov-Bohm phase, what would happen if one were to replace the *charged* particles inside the SQUID by *neutral* particles? Is there some magnetic-like field leading to an analog of the Aharonov-Bohm effect, so that the neutral version of the SQUID can also sensitively measure this field? At that time, the answer seemed to be that the Lense-Thirring field of general relativity was this magnetic-like field. A natural extension of this question was: If one could sensitively measure *stationary* gravitational fields by means of quantum interference, could one also sensitively measure *time-varying* gravitational fields, i.e., gravitational radiation? One answer: The quadrupole (or tidal) symmetry of gravitational radiation would require that the neutral SQUID be twisted into a figure-8 shape before it could detect such radiation (see figure 4(b)).

Since the neutral SQUID, viewed as a macroscopic quantum system, would become, for weak gravitational fields, *linear and reciprocal* in its response to GWs, the question naturally arose: Could this figure-8 antenna also *generate*, as well as *detect*, GWs? Recently, RYC suggested a simplification of these earlier ideas, which eliminated the hard-to-make Josephson junctions [17]. Quantum systems such as the quantum Hall fluid, a *ferromagnetic* material that responds linearly and reciprocally to external perturbations, could lead to a kind of 'quantum transducer action', in which conversion of GWs into EM waves, *and vice versa*, could in principle occur. This coupling originates from an extension of the usual minimal coupling rule to include the coupling of spin to curved spacetime [17].

For example, the spin of the electron in a quantum Hall fluid can be viewed as a handle, by which it can be twisted around periodically in direction by a GW, thus causing it to pick up a periodic Berry phase. (The electron spin, which is a gyroscope-like object, locally undergoes *parallel transport* in the presence of a GW.) The Berry phase in turn induces macroscopic quantum flows in this charged quantum fluid which radiate EM waves. This *macroscopic quantum* process, in which a GW generates an EM wave, is *both linear and reciprocal*. Because of time-reversal symmetry, the time-reversed process in which an EM wave generates a GW, must also occur with equal power conversion efficiency; this efficiency can be at most unity [18]. This reciprocity principle suggests the possibility of a Hertz-like experiment for both generating and detecting high-frequency GWs, in which, for example, microwave EM radiation is first converted into a GW by one sample of the quantum fluid, and then the generated microwave GW is back-converted into EM microwaves by a second sample of the same quantum fluid. (Faraday cages would prevent the usual EM coupling between the generation and detection parts of the apparatus.) A first attempt at this type of Hertz-like experiment was performed using YBCO, a superconductor instead of a quantum Hall fluid, at liquid nitrogen temperature as the quantum sample [20]. An upper limit on the power conversion efficiency for the quantum transducer action of the YBCO sample was placed at 15 parts per million. YBCO is a zero-spin superconductor, however. Better choices might have been non-spin-zero materials like the spin-triplet superconductors, such as Sr_2RuO_4 [21], or the ferromagnetic superconductors, such as URhGe [22].

2 Matter-wave interferometry

Our primary motivation for studying GWs and their interaction with matter on the quantum level is based on the observation that matter-wave interferometers can be very sensitive detectors of GWs from astrophysical sources. The rest of this paper will be focus on demonstrating this sensitivity, and exploring the suitability of using matter-wave interferometers to construct MIGO, the *M*atter-wave *I*nterferometric *G*ravitational-wave *O*bservatory.

The gain in sensitivity expected in using matter-wave interferometry instead of laser interferometry in detecting GWs can be seen from the following argument: Roughly speaking, since an atom with mass m 'weighs' much more than a photon with frequency ω_γ, all other things being equal, a matter-wave-based Sagnac interferometer will be $mc^2/\hbar\omega_\gamma \sim 10^{10}$ times more sensitive as an inertial sensor of Earth's rotation than a light-wave-based interferometer [23]. This fact is well known [24], and the advantage of an atom-based Sagnac interferometer over a laser gyroscope has recently been shown experimentally [25, 26]. Although other important factors will also play a role, the inherent advantage of matter-wave interferometers over light-wave interferometers is expected to be pervasive, and not restricted only to the Sagnac interferometer.

Matter-wave interferometry is based on the particle-wave duality of quantum mechanics. This duality states that any massive object, such as an atom, can, under certain circumstances, behave like a particle, but can, under different circumstances, behave like a wave with a deBroglie wavelength $\lambda_{dB} = 2\pi\hbar/mv$, where v is the speed of a nonrelativistic ($v << c$) object. Like the phase of light, the *quantum* phase of an atom can be used to construct an interferometer using atoms, and we shall show that very sensitive observatories for GWs, which are expected to be many times smaller than corresponding light-wave-interferometer-based GW observatories such as LIGO (*L*aser *I*nterferometer *G*ravitational-wave *O*bservatory) and LISA (*L*aser *I*nterferometer *S*pace *A*ntenna), can be constructed with matter-based interferometers.

We shall argue here that the rapid technological advances in AMO physics that have occurred since the pioneering [27] work on atom interferometry have now made it possible to construct MIGO. These technologies did not exist in the 1970s and 80s when LIGO was first conceived and developed (see [7] for a history of LIGO); the inherent advantage of matter-wave interferometers over light-wave ones—suggested by the factor $mc^2/\hbar\omega_\gamma \sim 10^{10}$—either was not widely known or was not appreciated. Yet due in great part to this factor, MIGO can not only be many times smaller than either LIGO or LISA, but can also expand the frequency response range of current GW observatories to presently inaccessible regions, and can substantially extend the observational reach of GW observatories as well. It will also be possible to measure with MIGO other general relativistic effects that are not accessible to LIGO or LISA.

The study of matter-wave interferometry in connection with GWs was started by Linet and Tourrenc [28]. A few years later, Stodolsky also studied matter-wave interferometry and its use in measuring general

relativistic effects, including the detection of GWs. Both of these studies were done on the quantum mechanical level, and used as their underlying basis the *geodesic* equation of motion, not the geodesic *deviation* equation of motion, to calculate the phase shift of individual particles in both stationary spacetimes, and spacetimes with GWs. These works were complementary to those by Anandan [30, 31, 32], who focused more on matter-wave interferometry in stationary spacetimes and the Sagnac effect. He also used the quantum mechanical framework based on the geodesic equation. More recently, statements of the impracticality of using atom interferometry to detect GWs have been made by Kasevich and coworkers [25]. Studies of GW antennas using quantum condensed matter systems such as superfluids have also been done, and were started by Anandan and Chiao [33]. The extension of the quantum-mechanical-based analysis to a quantum-field-theoretic approach for spin-zero particles was done by Cai and Papini [34]. Later, Bordé and coworkers, in a series of papers [35, 36, 37], revisited the question of matter-wave interferometry and the measurement of gravitational effects—both stationary and nonstationary—using also quantum-field-theoretic methods, but now with the Dirac equation on curved spacetimes for a spin-half particle as their starting point. All of these quantum-field-theoretic approaches nevertheless resulted in a phase shift that is similar to Linet-Tourrenc's and to Stodolsky's.

What has not been well appreciated in the previous work in matter-wave interferometry and its use in detecting GWs is that gravity, unlike the other forces of nature, cannot be screened. Thus, when a GW passes through a system, say a matter-wave interferometer, the GW acts on *all* parts of the system. Consequently, only *differences* between particles can be measured [4, 12], and in the long-wavelength limit for GWs, the motion of particles is described by the geodesic *deviation* equation Eq. (3), and *not* by the *geodesic* equation on which previous analyses have been based. This fundamental feature of GWs is well known in the general relativity community, and is explicitly exploited in the design of both LIGO and LISA. In this paper, we will follow LIGO and the standard general-relativistic approach of using the geodesic *deviation* equation as a starting point in our analysis of matter-wave interferometry in connection with GWs. As a consequence, we arrive at an a phase shift for MIGO that is very much different than those calculated before based on the geodesic equation of motion. A detailed comparison of the approaches based on the *geodesic* equation, such as those listed in the above, versus our approach based on the geodesic *deviation* equation will be presented elsewhere [38]; we shall only present a general critique of the geodesic-equation approaches here.

Unlike LIGO, which uses laser interferometry to very accurately measure slight shifts in the *position* of a classical test mass—the end mirrors of the interferometer—when a GW passes by, MIGO measures slight shifts in the *velocity* of atoms caused by the GW. These velocity shifts in turn produces small changes in the deBroglie wavelength of the atom—a quantum test mass—and thus in its quantum phase. Like laser-based interferometers, these phase shifts can then be detected using interferometry, and we shall show that, assuming equal shot-noise limits,

$$L_{MIGO} \approx \left\{ 2B \left(\frac{\hbar \omega_\gamma}{mc^2} \right) \frac{c}{2\pi f L_{LIGO}} \right\}^{1/2} L_{LIGO}, \tag{4}$$

where L_{MIGO} is the effective size of MIGO, $B = 75$ is the number round trips the light beam takes within the Fabry-Perot interferometer placed in each arm of LIGO, ω_γ is the frequency of LIGO's lasers, m is the mass of the atom used in MIGO, f is the frequency of the GW, and L_{LIGO} is the physical length of one of LIGO's arms. At 125 Hz, where LIGO I, the current LIGO configuration, is most sensitive, $L_{MIGO} \approx 1.5$ m as compared to $L_{LIGO} = 4$ km if a ^{133}Cs atom is used [39]. Similarly, a comparison of a space-based MIGO with LISA leads to a MIGO configuration that is at least ten thousand times smaller than LISA, if they both have the same shot-noise sensitivity.

It should be emphasized that at a fundamental level MIGO measures the local Riemann curvature tensor *no matter what its source is*. This can most clearly be seen by drawing in *spacetime* the paths of an atom passing through an interferometer as was done in [42]; the two possible paths of the atom naturally forms a closed path in spacetime, similar to the ones is used to define the Riemann curvature tensor (see figure 1(b)). It is thus not surprising that like the well-known Berry's phase [15] and the Aharonov-Bohm effect for GWs [12], the Riemann curvature tensor encircled by the closed path induces a net quantum phase shift. However, for GWs we shall see that the additional action of the mirrors in MIGO on the atom produces a larger phase shift than that caused by the curvature tensor alone. Thus, in addition to detecting GWs, MIGO, unlike LIGO, will also be able to measure directly the local Riemann curvature tensor from *stationary* sources such

as the Earth, Moon, and Sun for the first time, and it may also be possible to measure the Lense-Thirring field of the Earth as well.

The main objective of this paper is to present the following: The concept of MIGO along with its underlying theoretical framework; an outline of the design of two different types of MIGO configurations; a calculation of the expected sensitivities of these configurations; an assessment of their potential as gravitational wave observatories. We shall also argue as to the feasibility of constructing a MIGO. To this end, using our analysis of the underlying physics of MIGO, we have estimated the specifications of an interferometer that would be capable of measuring GWs, and have outlined the technologies that could be used in reaching them. What has *not* been done here is a complete analysis of the systematic errors of MIGO. Since such an analysis would depend crucially on the precise structure of the interferometer, it would not be fruitful to do this without at least a small-scale MIGO in hand. We have, however, estimated the *fundamental* limitations to MIGO's sensitivity due to thermal fluctuations of the mirror. Moreover, as we shall see below, the various technologies needed to construct MIGO have already been *separately* demonstrated in various atom diffraction and interferometry experiments since the early pioneering work in the 1990s. What has not been done is the integration of these components into a complete atom interferometer that has a design and a sensitivity to detect, measure, and observe GWs.

It is unfortunate that misconceptions of atom interferometry, on the one hand, and laser gravitational wave detection schemes, on the other hand, are prevalent among both the LIGO and the AMO communities. Among the AMO community, on the one hand, it is often believed that it is the light beams in the arms of LIGO's interferometer that is being acted upon by the GW; the mirrors plays little role. Precisely the opposite is true. In Thorne's 'proper reference frame', it is the action of the GWs on the end mirrors of the interferometer, which are suspended vertically with piano wires, that is being measured; light is used simply as a means to measure the shifts in the mirror's position. In addition, the AMO community often tries to understand the properties of GWs and their interaction with matter through an analogy with the gravitational redshift. This also is too naive. As we have described in the Introduction, GWs are a *dynamical* effect, while the gravitational redshift is a *static* effect. Attempting to understand the action of GWs on matter with the gravitational redshift is like trying to understand electromagnetic waves using only the scalar potential. Next, the fundamental difference between geodesic motion and geodesic *deviation* motion is not appreciated. In stationary spacetimes, such as that surrounding the Earth, a global coordinate system can be constructed, and the motion of test particles can be described using the geodesic equation [12]. In non-stationary spacetimes, such as when a GW is present, such a coordinate system cannot be constructed, and only the *relative* motion of test particles can be described, resulting, in the long-wavelength limit, in the geodesic *deviation* equation of motion.

Among the LIGO community, on the other hand, it is often thought that the use of atom interferometry to detect GWs simply involves replacing the light beams in LIGO with atomic beams. The gain in sensitivity is then only due to the shorter de Broglie wavelength of the atoms compared with the wavelength of the light currently used LIGO; it is still the motion of the mirrors that will be measured. This viewpoint also is too naive. Atoms are not photons, and their response to GWs is different than that of photons. As we shall see below, the *nonrelativistic* atoms used in MIGO are moving so slowly that it is the effect of the GWs on the speed of the *atoms* that will be measured; the motion of the mirrors are a secondary effect.

We hope that the pedagogical nature of this paper will dispel these misconceptions.

3 Background and Review of Research

3.1 Matter-wave Interferometry

We begin with a brief review of the physics underlying matter-wave interferometers. Detailed reviews can be found in [43, 44].

3.2 Principles of Matter-wave Interferometry

Matter-wave interferometry is based on the particle-wave duality principle of quantum mechanics, which states that every massive quantum object characteristics of both a particle and a wave. Which of these two

characteristics it exhibits depends on the properties an experimentalist wishes to measure or exploit. Using this principle, various interferometers have been constructed with a wide variety of sources, beam-splitters, mirrors and detectors (see [43, 45]). Following the COW [6] experiment in the 1970s, in the 1990s, Pritchard's demonstration of *atom* interferometry [27] using sodium atoms was followed shortly thereafter by the work of Chu and Kasevich [46] with cesium atoms, to perform extremely sensitive measurements of the local acceleration due to Earth's gravity. Subsequently, the phase shift of atoms caused by the Earth's rotation was measured not only with traditional Mach-Zehnder-type interferometers [25, 26], but also with ^{4}He and ^{3}He superfluid Josephson-Anderson junctions [47, 48] as well. More recently, matter-wave interference of fullerene (C_{60}) molecules has also been reported [49].

Because of the particle-wave duality, every particle possesses a deBroglie wavelength λ_{dB}, and, due to its wavelike nature, massive particles can be diffracted, reflected, and coherently beam-split—all the properties of light that are needed for light-wave-based interferometry. However, *unlike* light, λ_{dB} depends explicitly on the *speed* of the particle, and its wavelength can be altered continuously. Just as important, a slowly moving massive particle responds to the presence of gravity much more sensitively than light, as we shall see below.

Like light-wave interferometry, matter-wave interferometers can be divided into three distinctive parts: the source emitting the interfering particle, the 'atom optics' consisting of beam-splitters and mirrors, and the detector. In a generic matter-wave interferometer a source emits particles—either in a continuous stream or in bunches—which is then split into two (or more) paths at the beam-splitters. (It is important that the particle beam is split *coherently* so that it is not possible—due to the superposition principle of quantum mechanics—to determine *which path* the particle will travel along.) Mirrors are then used to change the direction of the beams so that they are eventually recombined and detected. Like the beams of light in light-wave interferometers, the particles passing through the interferometer picks up a phase shift $\Delta\phi = \left(S_{cl}^{\gamma_1} - S_{cl}^{\gamma_2}\right)/\hbar$, but now $S_{cl}^{\gamma_1}$ and $S_{cl}^{\gamma_2}$ are the action for a particle travelling along the two *quasi-classical* paths γ_1 and γ_2 of the two arms of the interferometer.

3.3 Supersonic Sources

Supersonic sources were first developed in the 1960s by chemists for the study of chemical reactions (see Chapter 2 of [45]), and they have a number of properties superior to the effusive sources (ovens) that are more often used by physicists. While the velocity distribution of atom beams from effusive sources is essentially a Maxwellian one that is fixed by the temperature of the oven, the velocity spread of supersonic sources are much narrower. Fractional velocity spreads of 1%—0.3% for helium—has been achieved from continuous supersonic sources, and even smaller fractional velocity spreads can be achieved using pulsed sources. Nearly monoenergetic beams with very high intensities can thus be formed. Pritchard, for example, has produced 10^{21} atoms/cm^2/s/sr sodium beams [27], and Toennies has produced very cold helium beams with 1.5×10^{19} to 1.5×10^{20} atom/sr/s [50]. Throughputs of atoms, measured in atoms per second, in atom interferometers using supersonic sources are thus orders of magnitude larger than those obtainable using either effusive sources, such as those used by Kasevich [25, 26], or magnetic-optical-trap sources, such as those used by Chu [46]. In addition, by seeding the beam with the appropriate type of atom, the centreline velocity of the atomic beam from a supersonic source can be increased or decreased. This flexibility is another advantage that supersonic sources have over effusive sources.

3.3.1 Continuous Supersonic Sources and Optical Molasses Collimation

A typical continuous supersonic source functions as follows: A jet of gas from a high-pressure reservoir escapes supersonically in free expansion through a nozzle, consisting of a small orifice typically 10 to 100 microns in diameter, into a differentially pumped low-pressure chamber that has a larger orifice at its output end called the 'skimmer'. This skimmer has the appropriate geometry so that it can skim away the hotter outer components of the rapidly expanding gas jet, thus leaving only the intense, low-temperature, central component of the atomic beam to enter into another differentially pumped chamber. Importantly, after expansion, the collision times of atoms in the beam reduce dramatically, and effectively they no longer collide with one another. The beam is often further collimated by a slit at its output end, and it could be collimated yet again using a second slit at the output end of yet another differentially pumped chamber

before it enters the main vacuum chamber containing the atom-based device, such as an interferometer (see for example [27]). With successive stages of differential pumping, by means of either diffusion or turbomolecular pumps, one can maintain an ultra-high vacuum in the main chamber that is often needed. In addition, using optical molasses techniques [51], beam collimation can be achieved without throwing away most of the atomic beam, as is currently done when collimating slits are used. The combination of 2D optical molasses collimation with effusive sources has already been achieved by [25, 26]. Its combination with supersonic sources, as we propose here, can yield the high-brightness atomic beams necessary for a good signal-to-noise ratio in MIGO.

3.3.2 Pulsed Supersonic Sources and Optical Molasses Collimation

Most pulsed supersonic sources function in much of the same way as continuous supersonic sources, but with the addition of a fast-acting valve to pulse the beam. Duty cycles of roughly 10^{-4} can be achieved, and as a result, very high fluences can be obtained. Because of the short duty cycles, smaller vacuum pumps than those used in continuous supersonic sources can be used instead. Of particular interest is the pulsed source developed by Powers et. al. [52], which uses laser ablation of metallic sources such as lithium (see [53] for a review of laser ablation) to generate the atomic beam. The high-pressure gas chamber is replaced by the laser plus metal assembly. As before, optical molasses can be added to reduce the velocity spread, and thereby collimate the beam.

3.4 LIGO and the Detection of GWs

With the advantage of being a scalable design, the great majority of the current experimental searches for GWs are based on laser interferometers. A number of research groups located throughout the world [54] are expecting to begin to collect data soon: GEO600, a German-British collaboration; VIRGO, a French-Italian collaboration; TAMA300, a Japanese effort; and ACIGA, an Australian effort. LIGO, the US-based, international collaboration, is currently collecting data, and LISA, a space-based laser interferometer system, is currently in the initial planning stage. We shall focus primarily on LIGO in this paper.

LIGO is a set of three interferometers based at two locations—Hanford, Washington and Livingston, Louisiana—separated by 3020 km [55]. All three instruments are based on Michelson interferometers with Fabry-Perot arms. The physical length of the each arm of the main LIGO interferometer is 4 km, and the Fabry-Perot interferometer increases the optical path of the arm a factor of $2B = 150$. In its current LIGO I configuration, a 8 W Nd:YAG laser is used with $\lambda_\gamma = 1.064$ μm. At the end of each arm is a massive mirror suspended vertically within a vacuum chamber; the location of the mirror assembly for the end mirror must be held in position within 10^{-10} to 10^{-13} m with respect to the central beam splitter of the interferometer. As we shall see in the next section, the passage of a GW through the interferometer shifts the position of the end mirrors, thereby causing a net phase shift of the light, which is then measured. The laser interferometer used by LIGO thus provides the means of accurately measuring the position of the mirrors over a large distance.

While each end-mirror could be fixed to the mirror assembly, the end mirrors would, through their connection with the mirror assemblies, be mounted to the ground below. The response of the interferometer to the passage of the GW would then depend on the material properties of both the ground and the frame of the interferometer across the 4 km spanned by LIGO's arms. Thus, by fixing the mirrors to the mirror assemblies, one ends up measuring the response of the *Earth* to the GW, and not of the mirrors. If this is done, sources of systematic errors—such as changes to the material properties in the Earth along LIGO's arms—cannot be controlled. Consequently, instead of fixing the end mirrors to the mirror assembly, they are suspended on piano wires, and are thus decoupled as much as possible from sources of uncontrollable systematic errors. Even so, at frequencies below 125 Hz thermal noise in the piano wires will begin limiting LIGO's sensitivity, and below 40 Hz, seismic noise causes a rapid decrease in sensitivity. At frequencies above 125 Hz, shot noise begins limiting the phase sensitivity of the interferometer.

Construction of LIGO began in 1996, and the main interferometers were commissioned in 2001 [55]. The first science runs were started in June of 2002, and these data are currently being analysed. The installation of LIGO II—designed to be used for GW astronomy—is expected to begin in 2006.

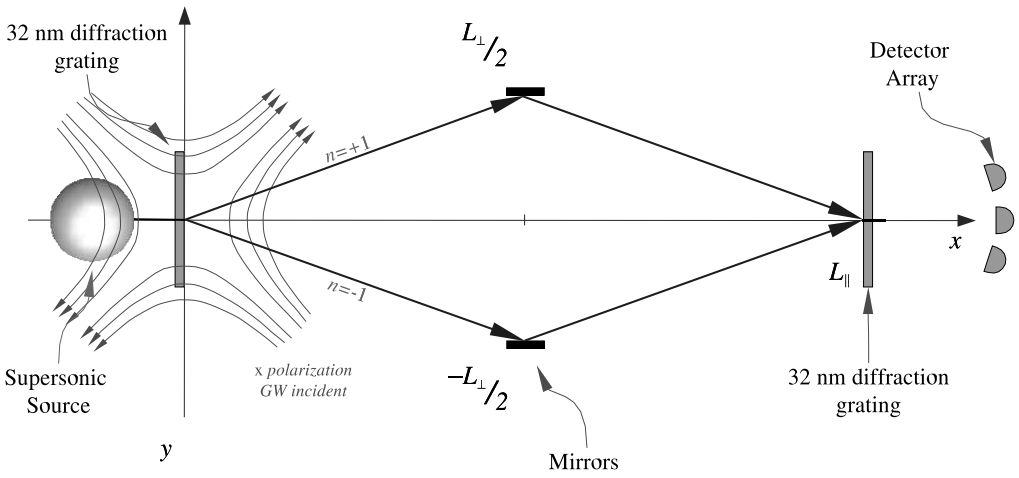

Figure 5: Schematic diagram of the horizontal MIGO configuration, with a GW incident normal to the plane of the interferometer. Only the $\times$ polarization contributes to the phase shift; the $+$ polarization does not. Diffraction orders other than $n = \pm 1$ are left out for clarity.

4 A *M*atter-wave *I*nterferometric *G*ravitational-wave *O*bservatory (MIGO)

In this section we outline two possible configurations of MIGO and the technologies that could be used to construct them. We also derive the phase-shifts expected for this MIGO, and use this calculation as a guide in determining the specifications of MIGO based on current technology.

4.1 Theoretical Basis

In this subsection we outline the physics underlying LIGO and MIGO, and demonstrate that they are both based on the same underlying physics, one at the classical level, the other at the quantum level. The treatment here will be semi-quantitative, and will focus on the fundamental physics. A complete derivation of MIGO's phase shift is given in **Appendix B**, and the reader is referred to [7] for the derivation of LIGO's phase shift. Like LIGO, we construct our coordinate system along the lines given in the Introduction (see [12] as well), and we measure the position and movements of particles with respect to the initial beam splitter (see figures 5 and 6).

The basic physics underlying LIGO is as follows: Since the mirrors at the end of each of LIGO's arms are hung as pendula with piano wire, they are free to oscillate along the interferometer's beam line. As a GW passes through the interferometer it slightly shifts the position of both mirrors by a small amount Δx. This in turn causes a shift $\Delta\phi_{LIGO} = 2\pi B\Delta x/\lambda_\gamma$ in the phase of light (with wavelength λ_γ) used in the interferometer [7, 56]. (The restorative force of the pendula on the mirrors can be neglected here.) It is thus

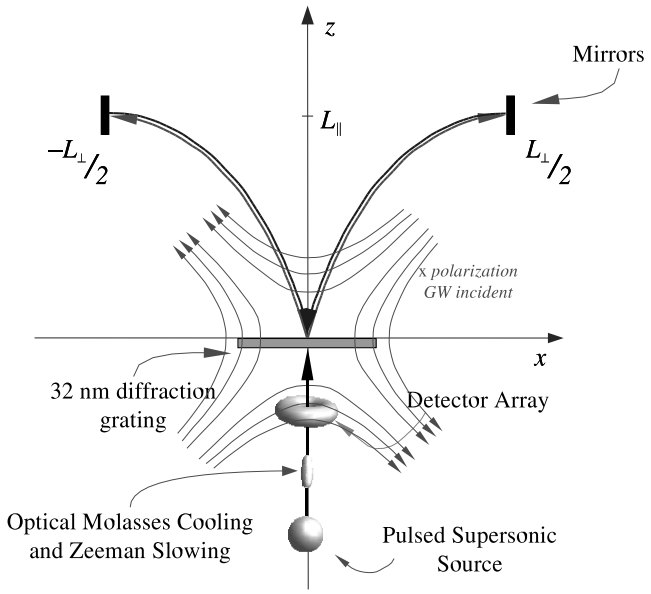

Figure 6: Schematic diagram of the vertical MIGO configuration, with a GW incident normal to the plane of the interferometer. Only the $\times$ polarization contributes to the phase shift; the + polarization does not. Diffraction orders other than $n = \pm 1$ are left out for clarity.

the shifts in the position of the *mirrors* caused by the GW that is being measured, and not the changes caused by the GW in the properties of the *light*, as it is often thought among the AMO community. The light used is only a very accurate means of measuring shifts in the mirror's position.

As described in the Introduction, the motion of the mirrors in the interferometer is govern by the geodesic deviation equation Eq.(3). Since the passage of the GW causes only a small change in the position of the mirror, $\Delta x \approx L_{LIGO} h_+/2$ where $L_{LIGO} = 4$ km is the physical length of an arm of LIGO, and h_+ is the amplitude of the + polarization of the GW; the $\times$ polarization does not affect the motion of the mirrors appreciably. This shift in the mirror's position changes the optical path length of the interferometer, and causes a phase shift in the light used in the interferometer given by $\Delta\phi_{LIGO} = 2\pi B L_{LIGO} h_+/\lambda_\gamma$ [56, 7]. The factor B is the number of round trips that the light beam makes inside the Fabry-Perot interferometers in LIGO's arms. Strictly speaking this expression for $\Delta\phi_{LIGO}$ is only applicable for GWs with frequencies ~ 125 Hz; at 4 km, the arms of LIGO is equal to the reduced wavelength of a GW in the upper end of its frequency response spectrum, and causality has to be taken into account (see [57], page 550). While design characteristics of LIGO, such as power recycling and shot-noise modifications by the Fabry Perot arms, will change the sensitivity from this simple form, it is accurate enough for our purposes in this section.

If the phase shift for LIGO is proportional to the length of its arms, how, then, does the phase shift for MIGO depend on its size? Figures 5 and 6 are drawings of two possible configurations for MIGO with the force-field lines of a $\times$ polarization GW drawn in at the origin of our coordinate system. A complete description of these configurations will be given in the next subsection. For now, we note that on a classical level, the motions of the atoms used in MIGO are governed by Eq. (3) as well. However, while in LIGO

one considers shifts of a mirror's *position* placed at a distance from the central beam splitter (which is the origin of LIGO's coordinate system) due to the passage of a GW, in MIGO one considers shifts in an atom's *velocity* as it travels through the interferometer due to the GW. Thus, while an atom may have an initial *velocity* v_0^i after it passes through the first beam splitter (in contrast with the end mirror in LIGO which has an initial *position*), the passage of a GW will cause this velocity to be shifted by an amount roughly $\Delta v^i \sim v_0^j \dot{h}_{ij} T/2$ after it has traversed the length of the interferometer in a time T. With a typical $|h_{ij}| \sim 10^{-20}$, this velocity shift of the atoms is extremely small, and must be measured on the quantum level by means of matter-wave interferometry.

Note that the tidal force-field lines sketched in figures 5 and 6 break the bilateral symmetry of the interferometers. It is this breaking of the bilateral symmetry by a $\times$ polarization GW that leads to a non-zero phase shift.

Changes in the atom's speed $|\Delta v|$ result in changes to its deBroglie wavelength, and hence to cumulative changes in its quantum phase. Indeed, since the change in the atom's position due to this speed shift after it passes through the interferometer is roughly $\Delta L_{MIGO} = 2|\Delta v^i| T \sim L_{MIGO} T \left|\dot{h}_{ij}\right|$ (the factor of 2 comes from having two arms in the interferometer), where L_{MIGO} is the effective size of MIGO, and the transit time $T \sim L_{MIGO}/|v_0^j|$. Like a laser interferometer this change in position will cause a phase shift, $\Delta\phi_{MIGO} = 2\pi \Delta L_{MIGO}/\lambda_{dB} \sim m L_{MIGO}^2 |\dot{h}_{ij}|/\hbar$, where the *deBroglie* wavelength of the atom is now used instead of the wavelength of light. Thus, in contrast to LIGO's phase shift $\Delta\phi_{LIGO}$, which is proportional to h_{ij}, MIGO's phase shift $\Delta\phi_{MIGO}$ is proportional to the *rate of change* of the GW amplitude $\dot{h}_{ij} \sim f h_{ij}$.

Although simplistic, this rough derivation of the MIGO phase shift nevertheless elucidates the underlying physics of MIGO. The above expression for the MIGO phase shift is close to the exact equation calculated in **Appendix B** after a detailed analysis of the MIGO configurations shown in figures 5 and 6,

$$|\Delta\phi_{MIGO}(f)| = 2\pi \frac{m}{\hbar} A f h_\times(f) |F(fT)|, \tag{5}$$

were $A = L_{MIGO}^2$ is the effective area of the interferometer, m is the mass of the atom, f is the frequency of the GW, and $h_\times$ is the amplitude of the $\times$ polarization of a GW. Equation (4) follows from Eq. (5), the above expression for $\Delta\Phi_{LIGO}$, taking $|F(fT)| \approx 1/2$ for freely suspended mirrors, and setting the shot-noise limits of the phase shift of MIGO equal to that of LIGO. The resonance function $F(fT)$ depends on the specific configuration of the interferometer, and measures the resonances between the GW and the interferometer. Precise forms for A and $F(fT)$ are given in **Appendix B**. The corresponding shot-noise-limited sensitivity for MIGO is

$$\tilde{h}(f)_{shot}^{MIGO} = \frac{\hbar}{2\pi m A f |F(fT)| \dot{N}^{1/2}}, \tag{6}$$

where $\dot{N}$ is the number of atoms passing though the interferometer per second. In comparison

$$\tilde{h}(f)_{shot}^{LIGO} = \left\{\frac{\hbar\omega_\gamma}{2 I_o \eta c}\right\}^{1/2} \frac{2\pi f}{\omega_\gamma}, \tag{7}$$

where I_o is the power of the laser, and η is the photodetector efficiency (Eq. 123a of [7]). Thus, while $\tilde{h}(f)_{shot}^{LIGO}$ *decreases* at higher frequencies, $\tilde{h}(f)_{shot}^{MIGO}$ *increases*. This complementarity between the two sensitivities is due to a fundamental difference in the signals being measured by LIGO and MIGO: LIGO measures the *position*, while MIGO measures the *velocity* of test masses.

Unlike LIGO, MIGO is only sensitive to the $\times$ polarization, not the + polarization. Also, while the phase shift of LIGO scales with its *length*, the phase shift of MIGO scales with its *area*; the larger the area, the smaller the amplitude of the GW that can be detected. When the transit time is much greater than the period of the GW, $|F| \sim 1/2$ for freely suspended mirrors; $|F| \sim \pi f T$ when it is much less than the period. What is not included in Eq. (5) is the Sagnac effect caused by the rotation of the Earth [25, 26], and the phase shift caused by stationary sources of curvature such as the Earth. While for the configurations shown in figures 5 and 6 these phase shifts are expected to be very large, they are, however, steady-state, and thus can be isolated from the time-varying signal caused by a GW.

4.1.1 Slow Atoms and the Response of MIGO

With the characteristic speed of an atom from a supersonic source being in the hundreds of meters per second range, and T in the range of seconds, we would naively expect MIGO to respond very slowly to the passage of a GW, which moves through the interferometer at the speed of light. (However, even for a laser-interferometer-based observatory such LIGO, which has arms that are roughly equal to the reduced wavelength of a 10^4 Hz GW, the transit time of light through LIGO is comparable to the period of the GW as well.) Because of the cumulative effect of the GW on the phase of the atom, we would expect $\Delta\phi_{MIGO}$ to be the result of averaging the phase of the atom over many periods of the GW, and thus to be close to zero. This does not happen for the following two reasons.

Firstly, half-way through the interferometer the atoms in the beam hit, and are reflected off, a set of mirrors. These mirrors impart on the atoms an *instantaneous* force whose strength is proportional to the *instantaneous* velocity—including the changes to the atom's velocity caused by a GW as it travelled between the beam splitter and mirror—of the atom normal to the mirror. From the force-field lines drawn in figures 5 and 6, the magnitude of this force will be different for atoms travelling along the $n = +1$ and $n = -1$ paths, and they will induce a net phase shift between the atom travelling along the two different paths. This can be seen explicitly in the derivation of the MIGO phase shift given in the **Appendix B**, where the force that the mirrors exert on the atoms results in a jump condition for the atom's velocity in the direction perpendicular to the mirror's surface. For high-frequency GWs this effect of the mirror's impulsive force is the dominant contribution to $\Delta\phi_{MIGO}$, and is the reason why $|F| \sim 1/2$ for freely suspended mirrors when T is much longer than the period of the GW. At lower frequencies, when T is much shorter than the period of the GW, the mirror's impulsive effect is very much reduced.

Secondly, notice from Eq. (3) that due to the *tidal* nature of the GW, its effect on the motion of the atom *increases* as the atom moves away from the beam splitter; the atom 'sees' a larger effective acceleration later in its path through than interferometer than it did at the beginning. Although for low frequency GWs this results in a relatively small resonance function $|F| \sim \pi f T$, the phase shift nonetheless does not average out to be zero as quickly as one might expect.

The relative sizes of MIGO compared with LIGO given by Eq. (4) would also seem to be counterintuitive. MIGO makes use of slowly-moving, nonrelativistic atoms to make its measurements, while LIGO would seem to make use of photons moving at the speed of light c. At first glance it would seem that MIGO should be *less* sensitive to GWs than LIGO by some power of v_{atom}/c. This, however, would be an erroneous argument. As outlined in **3.4**, it is *not* the effect of GW on the *light* used in the laser interferometer that is being measured in LIGO; it is the effect of the GW on the *test masses* (the *end mirrors*), *which are at rest*, that is being measured. Indeed, it is precisely because the atoms are *slowly moving*, i.e., *nonrelativistic*, that the effect of GWs on their motions are much more readily measurable than their effect on light. A GW can readily change the speed of nonrelativistic atoms, but it cannot change the speed c of light.

As a consequence, we would expect the *slower* the atom is, the more *sensitive* MIGO will be, as long as the atoms in the beam do not decohere because of long transit times through the interferometer. As counterintuitive as this conclusion may be, it can be arrived at through the following thought experiment. Suppose we replace the slowly moving, nonrelativistic atoms in MIGO by a series of faster and faster atoms until the atoms in the beam approach the speed of light. In this ultrarelativistic limit, the atoms behave much like the light used in LIGO, and it is apparent the horizontal MIGO configuration would be similar to LIGO, but with mirrors that are rigidly attached to the frame of the interferometer, instead of the freely moving mirrors in LIGO. Since it is well known that the sensitivity of LIGO decreases greatly if rigidly mounted mirrors are used instead of suspended ones, MIGO's sensitivity to GWs when ultrarelativistic atoms are used is expected to be much worse than if slowly moving atoms are used. Seen another way, because the speed of ultrarelativistic atoms are so close to the speed of light, changing their speed by even a small amount requires a great deal of energy. The speed of nonrelativistic atoms, on the other hand, are much more readily changed, and for the same amount of energy, a GW can shift the speed of a slow, nonrelativistic atom much more than the speed near c of an ultrarelativistic one, and thereby can cause a much larger phase shift for the nonrelativistic atom. To summarize, we would expect that the sensitivity to detecting GWs to *decrease* if ultrarelativistic particles—which behave like photons—are used in MIGO instead of slowly moving, nonrelativistic atoms. However, the slowly moving atoms must not decohere due

to collisions during the transit times through the interferometer.

4.1.2 Comparing MIGO with Other Approaches to the Detection of GWs using Matter-wave Interferometers

Equations (4), (5), and the conclusion that the sensitivity of atom-based interferometers to GWs is *larger* in comparison to light-based interferometers, are also surprising when compared to the results of Linet-Tourrenc [28], Stodolsky [29], Cai-Papini [34], and Bordé and coworkers [35, 36]. Complete criticisms of these approaches will be given elsewhere [38]. We note here simply that the approaches taken by both Linet-Tourrenc and Stodolsky have their roots in the *geodesic* equation of motion. Linet-Tourrenc used the quasi-classical approach based on the relativistic single-particle Hamiltonian for a relativistic particle derived from the geodesic equation; Stodolsky based his approach on the relativistic single-particle action. Both authors do not explicitly define their coordinate systems. They both find a phase shift of the form

$$\Delta\phi_{geodesic} = \frac{c^2}{\hbar}\int_\gamma h_{ij}p^i p^j \frac{dt}{E}, \tag{8}$$

from the equation above Eq. (6.1) of [29], and Eq. [3.2.3] of [28]. (To conform with standard units, we have restored the requisite factors of c and $\hbar$.) The integral is over a closed path γ in spacetime that the particle takes through the interferometer, p_i is the momentum of the particle, and E is its *total* energy including the rest mass. In comparison, if we also, for the moment, neglect the action of the GW on all parts of the interferometer (which is an unphysical assumption), we find the change in the action to be

$$\Delta\phi_{geodeviation} = \frac{m}{\hbar}\int_\gamma dt\left(\frac{1}{2}\vec{v}^2 - \frac{1}{2}\frac{dh_{ij}}{dt}x^i v^j\right). \tag{9}$$

The difference between $\Delta\phi_{geodesic}$ and $\Delta\phi_{geodeviation}$ is readily apparent, especially when the nonrelativistic limit of $\Delta\phi_{geodesic}$ is taken. $\Delta\phi_{geodesic}$ depends on the momentum of the particle and is independent of the length of the path travelled. Because of this momentum dependence of $\Delta\phi_{geodesic}$, it is expected that matter-wave interferometers will become more sensitive the closer to the speed of light the atom moves; i.e., the more ultrarelativistic the particle becomes, the larger its phase shift. This can be seen explicitly when the nonrelativistic limit of Stodosky's expression (Eq. (6.1)) for the phase shift of his interferometer is taken, in contrast to our expression for the phase shift of MIGO. On the other hand, $\Delta\phi_{geodeviation}$ increases linearly with the separation x^i, as it should, and the *larger* the interferometer, the larger the change in the phase, in agreement with the *tidal* nature of GWs. This linear scaling of the phase shift with the size of the interferometer is also a result on which LIGO is based. In addition, unlike previous studies, the effects of the mirrors on the atom's phase shift was also considered in our analysis. As a consequence, the phase shift of MIGO calculated in this paper has a dependence on the velocity of the atoms in the interferometer that is *opposite* from what Stodolsky calculated, when the nonrelativistic limit of his Eq. (6.1) is taken.

It should be emphasized that the differences between $\Delta\phi_{geodesic}$ and $\Delta\phi_{geodeviation}$ is due to more than the fact that one was derived in a nonrelativistic framework, and the other within a relativistic one. This can be seen by comparing the equations of motion for the particle used in the two approaches. Both Linet-Tourrenc and Stodolsky's approaches use the geodesic equation of motion, which, when GWs are present, becomes

$$\frac{d^2x_i}{dt^2} \approx -\frac{1}{2}\frac{dh_{ij}}{dt}v^j, \tag{10}$$

instead of the geodesic *deviation* equation Eq. (3). It is, however, well known that GWs affect *all* parts of the system, and since only *differences* in positions can be measured, it is the geodesic *deviation* equation that should be used, and *not* the geodesic equation. This becomes apparent in Eq. (10) with an acceleration for the particle dependent on the derivative of h_{ij}, and thus, from Eq. (15), on the connection. Equation (10) is thus a *frame-dependent* quantity, and will only have meaning only when a coordinate system is explicitly chosen. This choice was not explicitly made either by Linet-Tourrenc or by Stodolsky [58], nor by Cai-Papini or by Bordé and coworkers. This coordinate choice *is* explicitly made, and is well defined, in the derivation of the geodesic *deviation* equation of motion, Eq. (3), and is the reason why the acceleration

of the particle here depends on the Riemann curvature tensor, a frame-*independent* object. These are the underlying physical reasons why the above authors obtained the incorrect expression for the phase shift.

On the quantum-field-theoretic level, Bordé and coworkers start with the Dirac equation in curved spacetime. They used the standard formalism for quantum field theory in the presence of linearized gravity to study the phase shift that a GW induces on a generic atom interferometer using nonrelativistic, spin-half atoms. They obtained an expression (Eq. (92) of [35]) for the quantum phase shift of the atom that has a power-law dependency on $\lambda_{\perp dB}$ and λ_{GW} that is very much different than ours, and instead is similar to Linet-Tourrenc's and Stodolsky's. This also led them to the erroneous conclusion that atom-based interferometers are at best no more sensitive to GWs than light-based interferometers. Recall from Eq. (3), that the *tidal* effects of a GW on an atom *increases* with the separation distance between the observer and the atom. Bordé's governing Hamiltonian (Eq. 89 of [35]), on which their analysis was based, does not include these tidal effects of GWs, resulting in an incorrect expression for the quantum phase shift for the atom.

4.2 Description of MIGO Configurations

The two configurations of MIGO shown in figures 5 and 6 represent two possible operating extremes. In the horizontal configuration shown in figure 5, atoms are emitted from a continuous supersonic source with a velocity high enough that the acceleration due to Earth's gravity does not appreciably alter an stom's path by the time it traverses the interferometer. Indeed, not shown in the figure is a Zeeman laser *accelerator*, working oppositely to a Zeeman slower [51], that can accelerate the alkali atoms to even higher velocities. The atomic beam from the supersonic source is automatically collimated, and the distribution of velocities of the atoms in the beam transverse to the beam typically has a $\Delta v_t/v_s = 1\%$ for most atoms, and can be decreased to 0.3% for helium [45]. Alkali atomic beams from supersonic sources can then be further collimated by means of 2D optical molasses. The atom beam then passes through the first beam splitter, a nanofabricated transmission diffraction grating which, as with the diffraction of light, splits the beam into different diffraction orders n.

As shown in figure 5, only the $n = \pm 1$ orders are used here. In is important to note that the diffraction grating splits the atomic beam *coherently*. Consequently, from the superposition principle of quantum mechanics, *it is not possible to determine which path any one atom in the beam will take*; there is a finite probability *amplitude* it will take the $n = +1$ path, and due to the bilateral symmetry of the interferometer along the horizontal line, the same probability *amplitude* that it will take the $n = -1$ path. Irrespective of which path is taken, the most probable trajectory between the initial beam splitter and the mirror for the atom is determined by Eq. (3) (see [43] for the use of the Feynman path integral in atom interferometry). The mirror then reflects the atom by exerting an impulsive force whose strength is proportional to the velocity of the atom normally incident upon the mirror. (See [59] for recent advances in atom optics, such as coherent atomic mirrors made from crystals, and the possibility of using *curved* mirrors to coherently focus and collimate atomic beams.) Once again the most probable trajectory of the atom between the mirror and the final beam splitter—where the $n = +1$ path and the $n = -1$ path is recombined—is determined by Eq. (3); the atoms are then detected using standard methods [45]. In the absence of gravitational effects, the bilateral symmetry of the interferometer ensures that the $n = +1$ path will be the same as the $n = -1$ path, and no phase shift will be measured. This symmetry is broken when a GW is present, however; from the force-field lines drawn in figure 5, we see that path that the atom takes for the $n = +1$ order will be slightly different than the one taken by the $n = -1$ order, leading to MIGO's phase shift.

For the horizontal MIGO configuration, $A = L_\perp L_\parallel/2$—the actual area enclosed by the interferometer—in Eq. (5) (see **Appendix B**). Since the atoms travel in approximately straight lines through the interferometer, the length $L_\parallel$ of this MIGO configuration is determined by its width $L_\perp$, and the ratio of the horizontal velocity $v_\parallel$ of the atom to its transverse velocity $v_\perp$ after the initial beam splitter (see **Appendix B**). The sensitivity of a horizontal MIGO is thus proportional to $L_\perp^2$.

In the vertical configuration for MIGO shown in figure 6, alkali atoms are emitted from a pulsed supersonic source, and are then *slowed down* using a Zeeman slower [51] to velocities so slow that the acceleration due to Earth's gravity g now dominates the trajectories of the atoms through the interferometer, similar to the atom fountain geometry of Chu and Kasevich [46]. The beam is collimated using 2D optical molasses

as well [25, 26]. The velocity of the atoms v_s along the beam is slowed to such an extent that after passing through the initial beam splitter the atoms in the $n = \pm 1$ orders now traverse an almost parabolic trajectory to mirrors placed at the maximum height of their trajectories. The atoms are once again reflected at the mirrors, and fall back downward in an almost-parabolic trajectory where the paths are recombined by the same beam splitter, and subsequently detected. Once again, the *bilateral* symmetry of this interferometer along now the vertical line ensures that the gross motion of the atoms on the left side of the interferometer is reflected on the right side. The usual parabolic trajectories of the atoms is shifted slightly by an amount determined once again by Eq. (3) due to the passage of a GW, and will again be different for atoms travelling along the left hand path instead of the right hand path. It is this *asymmetrical* shift by the GW in the atoms trajectories that leads to the overall phase shift.

Similar to the horizontal MIGO configuration, $A = L_\perp L_\parallel$ for the vertical MIGO configuration as well (see **Appendix B**), but because the acceleration due to gravity g slows the atom down, it spends more time in the presence of a GW inside the interferometer than the atoms in the horizontal MIGO configuration do. Consequently, $L_\parallel = gL_\perp^2/8v_\perp^2$, where $v_\perp$, the horizontal velocity of atom after the beam splitter, is inversely proportional to the periodicity of the diffraction grating used. Thus, the area A is proportional to the *cube* of the width of the interferometer, and the sensitivity of the vertical MIGO configuration is proportional to $L_\perp^3$, and not to $L_\perp^2$ as for the horizontal MIGO configuration, or even to $L_\perp$ as it is for LIGO.

Like LIGO, both MIGO configurations make use of mirrors to redirect the atomic beams to beam splitters, and like LIGO, the response of MIGO to GWs will, to a certain extent, depend on how the mirrors are attached to the frame of the interferometer, and thus how the interferometer is attached to the Earth. However, because it is effects of the GW on the interfering particle, i.e., the atoms, that is being measured in MIGO, and not the mirrors as it is in LIGO, MIGO is much less dependent on how this attachment is made than LIGO is. Indeed, from **Appendix B**, we found that for $fT >> 1$, the response function $1/2 \leq F(fT) \leq 1$, irrespective of how the mirrors are attached to the interferometer. In fact, the *lower* limit of $1/2$ that is reached if the mirrors are freely suspended as in the case of LIGO, and the *upper* limit of 1 is reached if the mirror was firmly attached to an interferometer frame that can be approximated as infinitely rigid [60]. MIGO thus becomes more *sensitive* the more firmly the mirrors are attached to the interferometer frame. This is in direct contrast to LIGO, which become *less* sensitive. Indeed, if like MIGO we model the connection of LIGO's mirrors to the interferometer frame as a spring with resonance frequency f_0 and loss factor Q, we find from Eq. (37.16) of [4] that the shift in position of the end mirrors will be

$$\Delta x = \frac{f^2}{f^2 - f_0^2 + if f_0/Q} h_+ L, \tag{11}$$

In the limit where $f_0 >> f$, when the end mirrors can be approximated as mounted to an interferometer frame that is infinitely rigid, $\Delta x \approx 0$, and the LIGO looses all sensitivity to GWs.

From the sketch in figure 6 we see that the vertical MIGO configuration is a combination of Chu-Kasevich's atomic fountain interferometer with a Pritchard-type interferometer. Previous to Chu and Kasevich's work, Zacharias (see [61]) attempted to construct an atomic fountain in the 1950s and failed. Because of the effusive source used, there was a broad distribution of velocities in the atomic beam, and as the atoms in the beam climbed up the gravitational potential of the Earth, they started to slow down, and other, faster atoms started to overtake them. Scattering with the faster-moving atoms in the beam took place and coherence was lost. Chu and Kasevich avoided this by using laser-cooled atomic beams with narrower velocity distributions, as does MIGO.

4.3 Potential Sensitivity

The effectiveness of both MIGO configurations in detecting GWs can be seen in figure 7 where the characteristic amplitude and frequencies of GWs emitted from burst sources (the strongest emitters of GWs) such as supernova explosions and the coalescence of black holes, are plotted along with the amplitude and frequencies of the *smallest* of these types of signals that are detectable by MIGO, LIGO (both the current LIGO I configuration and the LIGO II configuration slated for operation in 2007), and LISA. Two of the configurations—the Earth-based vertical and horizontal—was designed to have a sensitivity equal to the best sensitivity of LIGO in its frequency range, and the third configuration—the Space-based horizontal—to have

a sensitivity equal to the best sensitivity of LISA in its frequency range. The signals from various classes of burst signals were replotted from Thorne's figure 9.4 [7]; the specifics of these sources can be found therein. The plots LIGO I, LIGO II and LISA have been updated from Thorne's original figure, and were generated from [7], [62], and [63], respectively, using Eq. 111 of [7].

All three graphs for MIGO were generated using Eq. (6), and a $\dot{N} = 10^{18}$ atoms per second (as compared with 8×10^{19} photons per second for LIGO). While $\dot{N} = 10^{18}$ atoms per second is very large, it is important to note that what is important is the *number* of atoms per second through the interferometer, and not the *number density*. Indeed, if the number density of atoms is too high, the atoms in the beam will condense, and beam coherence will be lost. By suitably constructing the supersonic source, and by choosing the proper operating regime for it, it may be possible ensure that the 10^{18} atoms per second needed to achieve figure 7 is spread over a large enough cross section of the beam to prevent condensation. We will comment further on this later in **4.4**.

A nanofabricated transmission diffraction grating with a periodicity of 32 nm was used in calculating figure 7. Although only reflection diffraction gratings with this periodicity have been made by the Nanoelectronic Research Centre at the University of Glasgow [64], by flipping the source and the detector array in figures 5 and 6, the MIGO configurations can be modified to use reflection gratings if transmission gratings cannot be constructed. As with LIGO, because GWs cannot be shielded, the passage of a GW through MIGO will shift all its parts, including the mirrors, and the response of the mirrors to the GW introduces an additional shift in the velocities of the atoms. However, since the mirrors in MIGOs do not have to be free to move, they can be constructed so that the effect of the GW on their motion is critically damped, as they were taken to be when figure 7 was graphed.

For the Earth-based vertical MIGO, bosonic ^{133}Cs atoms from a 2000 K continuous supersonic source are used in an interferometer with a width $L_\perp = 1.3$ m and a height of $L_\parallel = 237$ m. Zeeman cooling of the vertical velocity of the atoms from the beam is used to decrease the velocities of the atom by a factor of 11.6, and additional 2D optical molasses cooling is used to narrow by a factor of 10^4 the velocity of the atoms perpendicular to the beam. The Space-based MIGO, which is depicted as a horizontal configuration, also uses ^{133}Cs atoms emitted from a 2000 K continuous supersonic source, but with 2D optical molasses cooling used only to collimate the beam. As a result, while $L_\perp = 2$ m, the length of the interferometer is $L_\parallel = 17$ km, as compared to 5 million km for LISA. (Although a throughput of 10^{18} atoms/s is high for a space-based MIGO, atoms can be recycled from detector to source.) The final Earth-based horizontal MIGO graph also has a $L_\perp = 1.2$ m, but uses fermionic ^{6}Li atoms from a 2000 K supersonic source in conjunction with a Zeeman laser *accelerator* to increase the beam-velocity of the atom by a factor of 1.86. By angling the beam slightly upward, the maximum height of the beam as it travels across the length $L_\parallel = 4$ km of the interferometer is only 0.41 m; 2D optical molasses is used to collimate this beam as well. This MIGO configuration, while not optimal, is designed so that *whole* interferometer fits within one of the 1.2 m wide evacuated beam tubes that form the arms of LIGO. Enlarging sections of the beam tube to ~ 2 m will allow ^{133}Cs to be used instead of ^{6}Li, resulting in a 37-fold increase in the Earth-based horizontal MIGO sensitivity as shown in figure 7.

In figure 7 we see that by replacing the lasers in one of LIGO's arms with the ^{6}Li horizontal MIGO, the sensitivity of the GW observatory can be increased by a factor of 10. At 1.2 m $\times$ 237 m, the Earth-based vertical MIGO has the same sensitivity as LIGO II in its most sensitive frequency regime, while at 2 m $\times$ 17 km, the Space-based MIGO has the same sensitivity as LISA in LISA's operating regime. But all three MIGO configurations are sensitive to a much wider range of GW frequencies than LIGO and LISA, and they extend the range of GW observatories into frequency ranges—in particular between 0.1 and 10 Hz—not currently accessible by LIGO or LISA. In particular, note the sensitivity to high-frequency GWs of all three MIGO configurations graphed in figure 7, and the gradual *insensitivity* of LIGO to frequencies above 125 Hz and of LISA to frequencies above 2×10^{-2} Hz. This is due to the difference in the signal being measured by matter-wave-based and light-wave-based interferometers: MIGO measures shifts in the atom's *velocity*, and thus the *rate of change* of the GW amplitude with time; the larger the velocity shift, the larger the phase shift. This rate of change *increases* at higher frequencies, and is the underlying reason the smallest-amplitude GW that three MIGO configurations can detect in figure 7 *decreases* as $1/f^{1/2}$ at high frequencies. In contrast, LIGO (and LISA) measures the *position* of the end mirrors, which depends only on the amplitude of the GW, and only indirectly on its frequency. For the frequency of the GW to be

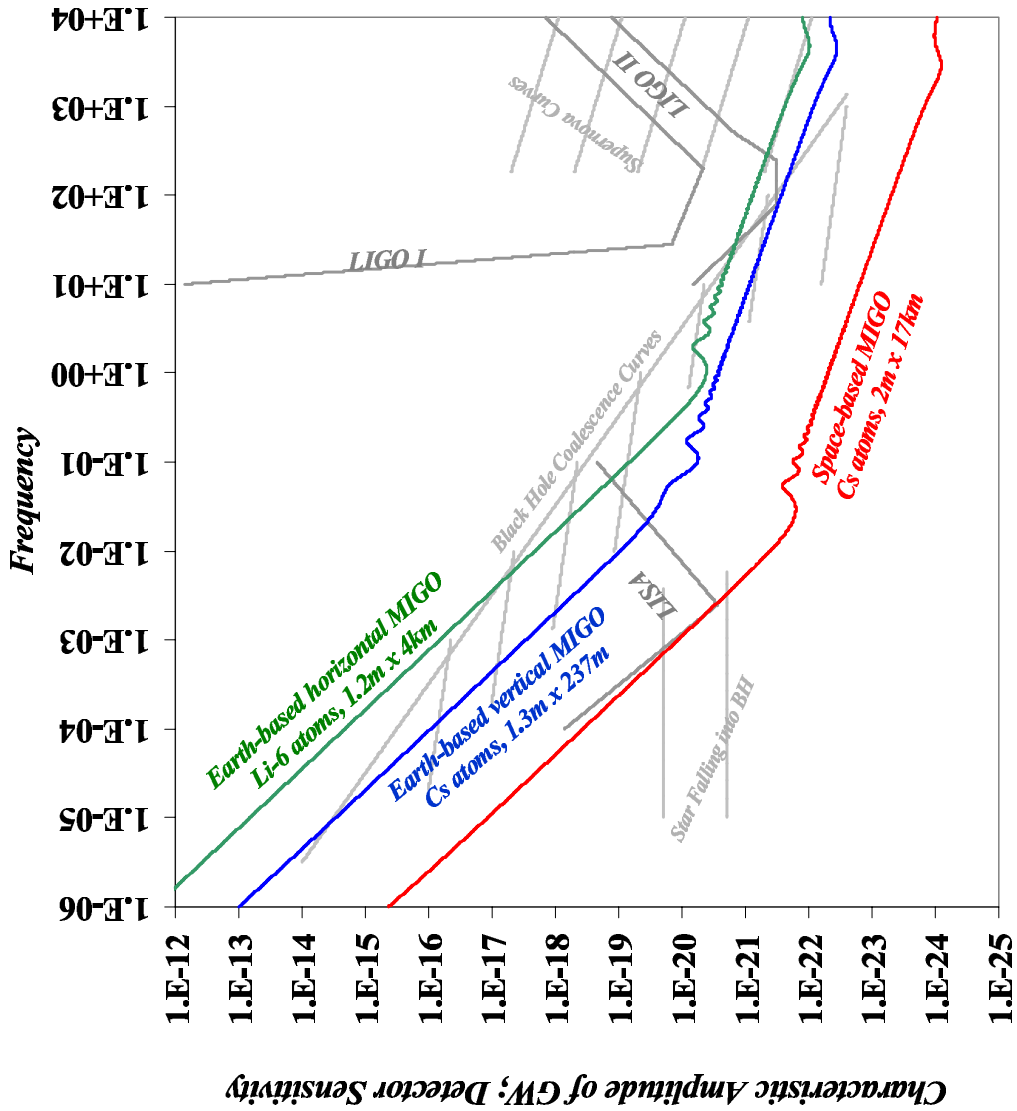

Figure 7: The ability of MIGO to detect GWs from various classes of burst sources is plotted, and compared with that of LIGO I [7], LIGO II [62] and LISA [63]. All three MIGO configurations are sensitive to a broad range of GW frequencies; they thus extend the range of GW observatories into frequency ranges not currently accessible.

measured, the smallest-amplitude GW that LIGO can detect must *increase* as $f^{1/2}$; it actually increases as $f^{3/2}$ because of shot-noise limits to $\Delta\phi_{LIGO}$. Indeed, if we compare shot-noise-limited sensitivities,

$$\frac{\tilde{h}(f)^{MIGO}_{shot}}{\tilde{h}(f)^{LIGO}_{shot}} \approx \frac{\hbar\omega_\gamma}{mc^2}\left(\frac{2\dot{N}_\gamma\eta}{\dot{N}}\right)^{1/2}\left(\frac{\lambda_{GW}}{2\pi L_{MIGO}}\right)^2 |F(fT)|^{-1}, \tag{12}$$

where $\dot{N}_\gamma$ is the rate at which photons enter LIGO.

4.4 Design Considerations

The inherent difference in the signal that they measure—MIGO measures *velocity* while LIGO measures *position*—impacts their constructions, and the fundamental limits to the size of the phase shifts both are capable of measuring. Both LIGO and MIGO will be subject to systematic errors arising from environmental perturbations, such as thermal and seismic noise; stray electric and magnetic field gradients; and fluctuations in g. Because the temperature of the beam splitters and the mirrors in both MIGO and LIGO cannot be zero, temperature-driven changes in their positions and velocities will induce thermal noise into phase shift measurements. Random seismic movement of the ground under the interferometer will introduce vibrational noise as well. However, while thermal noise starts limiting LIGO's sensitivity below 125 Hz and seismic noise effectively cuts it off below 40 Hz, their effect on MIGOs sensitivity is not nearly as great. Thermal and seismic noise have such a large effect on LIGO because LIGO's end-mirrors must be as close to a freely-falling mirror as possible. MIGO, on the other hand, makes use of beam splitters and mirrors that can be solidly mounted on an interferometer frame whose material properties can be well characterized and controlled, because of the relatively small size of MIGO. Standard vibrational isolation technologies can thus be used to minimize seismic noise to levels not attainable by LIGO; for these reasons seismic noise limitations are not shown in figure (7). However, temperature-driven oscillations on the surface of the mirrors—even though they are rigidly mounted—will induce random velocity (Doppler) shifts to the atoms, and subsequently random phase shifts. These oscillations, although not important for LIGO, will slightly affect the sensitivity of MIGO at very low frequencies. The effect of these oscillations on MIGO's sensitivity is estimated in **Appendix C**, and are included in figure 7. Unlike LIGO, the atoms in MIGO are subject to stray electric and magnetic fields. however, these effects can be made negligibly small with proper shielding and design. Fluctuations in g are due to density fluctuations caused by seismic waves, and will limit the low-frequency response of LIGO [73]. Its effect on MIGO is unknown, and can be eliminated with a space-based system.

At a fundamental level, unlike the photons used by LIGO, the atoms used in MIGO can interact among themselves; this requires a certain amount of care to be taken in the design of MIGO. Indeed, fermionic ^{6}Li was chosen for the Earth-based horizontal MIGO precisely because as a fermionic atom it will not scatter with other ^{6}Li atoms as readily as ^{7}Li, a bosonic atom, will. In this sense, cold, fermionic ^{6}Li atoms will behave more like the noninteracting photons in LIGO. Moreover, number squeezed states for fermions, which are very robust, can greatly reduce the shot noise of the atomic beam [39], [23]. This correspondingly reduces the required throughput of the atoms needed for the same sensitivity.

Any collision of the atoms within the beam—either with other atoms in the beam, or with stray atoms in the interferometer—will introduce random noise in $\Delta\phi_{MIGO}$, and decrease the contrast of the interference fringes. The cross-sectional area of the beam has to be made large enough, and the transverse velocity spread of the beam—narrowed using 2D optical molasses—has to be small enough that this does not occur within the transit time of the atom through the interferometer. Scattering with the background gas can be made negligible by using ultra-high-vacuum systems. Next, the supersonic source must be run at a high enough temperature that condensation of the gas of atoms into clusters—either solid or liquid—does not occur. At the same time, the pressure of the supersonic source must be high enough to generate a high intensity of atoms through the interferometer. Since we are dealing with atoms which can condense into liquids and solids, the allowed running temperature and pressure of the source will depend on the phase diagram of the atom, and the degree of supercooling of the gas that takes place. These issues are well studied for helium [65] (although they are not as well studied for the alkali atoms), and in general there does not seem to be a fundamental obstacle to finding a set of viable operating parameters. What is

more challenging is the throughput of 10^{18} atoms per second used in generating figure 7, which is close to the limits of current supersonic-source technology. However, because of the sensitive dependence of MIGO sensitivities on its size, a decrease in this throughput by a factor of 100 can be made up for by increasing the $L_\perp$ of a horizontal MIGO by a factor of $10^{1/2} = 3.16$, or that of a vertical MIGO by a factor of $10^{1/3} = 2.15$; decreases in the atom-beam throughput can thus be readily compensated for by modestly increasing the size of the interferometer.

At frequencies below roughly 125 Hz the sensitivity of LIGO decreases due to thermal noise, and radiation pressure on the end mirrors [62]. Photons in the laser impacting the mirrors not only exert pressure (and thus move) the mirrors, but because they are not perfect, the mirrors will be heated by the incident beam. Both factors will cause an overall decrease in LIGO's sensitivity. One would expect that since 10^{18} atoms per second should pass through MIGO to achieve high sensitivity, the impact pressure of the atoms on the mirrors, combined with the heating of the mirrors caused by the inelastic scattering of the atoms, would limit the sensitivity of MIGO as well. They do not for the follow reasons.

Quantum interference places stringent limits on the decoherence of the atom beam as it is diffracted from the beam splitters, and reflected off the mirrors. (Scattering of atoms in the beam off of background gas can be shown to be negligible.) In particular, it requires that there exists no possibility of 'which-path' information for the atom inside the interferometer. This in turn requires that diffraction of atomic beams off of beam splitters, and their reflection off of mirrors be elastic and coherent. *Consequently, an atom can only change the centre-of-mass momentum of the beam splitters or mirrors, and cannot deposit energy into them.* Since the mirrors and beam splitters of MIGO can be firmly mounted to the frame, the effects of this centre-of-mass momentum transfer can be minimized.

A measure of the inelastic versus elastic components of these processes is based on the Debye-Waller factor W through the intensity ratio $I/I_0 = \exp(-2W)$, where I is the diffracted (or reflected) intensity and I_0 is the incident intensity. The factor W is a measure of the fluctuations of the atoms in the crystal that diffracts the incident atomic beam. For diffracted atomic beams, $W = \mathcal{B}/a^2$, where a is the periodicity of the diffraction grating, and $\mathcal{B} \sim 0.5$ Å^2 at room temperature [66]. The rule of thumb [45] is that $W/12 < 0.1$, for sharp, elastic diffraction patterns to be seen. The requirement for observing interference is more stringent, however; the probability of emitting even a single phonon during the diffraction process must be negligible, and $W/12 < 0.01$ is required [67]. For nanofabricated diffraction grating and mirrors, $W/12 \sim 10^{-7}$ at room temperature and decreases at lower temperatures. Thus it is highly probable that the *zero-phonon* process is the dominant one, and therefore quantum phase coherence is expected in the interferometer.

As stringent as this zero-phonon-emission condition on atom interferometers may be, atom interferometers of the same type as MIGO have been successfully constructed before. For example, the interferometer used by Pritchard, which is very similar to the horizontal MIGO configurations, uses 1027 K sodium atom beams using 100 nm nanofabricated diffraction gratings. Both the temperature of the atoms and the size of the diffraction gratings are comparable to MIGO's. The fact that fringes have already been observed in Pritchard-type interferometers shows that decoherence due to the atom-beam-splitter interaction does not prevent interference from happening.

4.5 Measuring New General Relativistic Effects

The underlying advantages of MIGO over LIGO or LISA go beyond being smaller and more sensitive. It is also possible to explore with MIGO general-relativistic effects that are not accessible with LIGO.

4.5.1 Measurements of Stationary Riemann Curvature

As we have outlined in the Introduction, and have shown in figure 1(b), the parallel transport of a four-vector around a closed path is a measure of the local Riemann curvature tensor of the spacetime. Referring to figure 5, and extending the $n = \pm 1$ paths that an atom can take into spacetime, it becomes clear that in MIGO the atom does *precisely* what is indicated in figure 1(b): It is parallel transported around a closed path in spacetime, and as a result its phase is shifted by the local curvature of the spacetime [42] through an anholonomy. Although the delta-function impulsive forces in the mirrors impart an additional acceleration- and time-dependent phase shift to the atoms, the Riemann-curvature-tensor contribution still remains, and will be dominant for low-frequency GWs, and for stationary Riemann curvature tensors in general. It is thus

not surprising that MIGO is sensitive to the *total* local Riemann curvature tensor of spacetime, independent of its source, and not just the fluctuations caused by the passage of a GW, as LIGO is. Indeed, while in our analysis in **Appendix B** we have for clarity taken the acceleration due to gravity to be a constant—thus neglecting the contribution of the curvature from stationary sources such as the Earth—if we repeat the analysis focusing now for stationary gravitational fields we find that the horizontal MIGO configuration will measure a phase shift [42]

$$|\Delta\phi^{stat}_{MIGO}| = \frac{1}{2}\frac{m}{\hbar}L_{\perp}L_{\parallel}TR^{stat}_{0x0y}, \tag{13}$$

where R^{stat}_{0x0y} is the *total* local Riemann curvature tensor from stationary sources (once again the Sagnac effect is neglected). The Earth-based horizontal MIGO can thus measure $R_{0x0y} > 4 \times 10^{-24}$ s^{-2} in a one second integration time. With a local curvature of 1.23×10^{-6} s^{-2}, it will certainly be possible to measure the Earth's Riemann curvature tensor if the contribution from the Sagnac effect can be subtracted from the signal independent of the Earth's curvature's. It will also be able to measure the Riemann curvature tensor of the Sun ($|R_{0i0j}| = 3.2 \times 10^{-14}$ s^{-2}), and the Moon ($|R_{0i0j}| = 7.0 \times 10^{-14}$ s^{-2}) with MIGO; both curvatures vary predictably with time, and their signal can be discriminated from the static phase shifts cause by the Sagnac effect and the Earth. For comparison, a GW with an strain amplitude of 10^{-21}, and a frequency of 10^4 Hz from a supernova source shown in figure 7 has a rms $|R_{0i0j}| \sim 2.5 \times 10^{-14}$ s^{-2}, similar to the nearly static Riemann curvature of the Sun and Moon. If it is possible to subtract out both the Sagnac and Earth's curvature contributions, at a $|R_{0i0j}| \sim 1 \times 10^{-17}$ s^{-2}, the Earth-based horizontal MIGO will be able to measure the Lense-Thirring field of the Earth as well.

On a classical level, this Riemann-curvature-driven effect on the atom is surprising. In general relativity, an atom is modelled as a spin-zero, point-like test particle, and thus should not be directly affected by the curvature. However, on the quantum level the atom is described by a *delocalized* wavefunction ψ, which is a section of a $U(1)$ line bundle over the local spacetime manifold. Curvature-driven effects of the $U(1)$ fibers of the line-bundle above a *flat base manifold* is well known in quantum mechanics, and is the fundamental cause of Berry's phase [15, 17]. It should not be surprising that the Riemann curvature of a *curved base manifold* will cause phase shifts as well, in a gravitational version of the Aharonov-Bohm effect [12].

4.5.2 Spatial Variations of GWs

The length of LIGO's arms are such that $L_{LIGO} \leq \lambda_{min}/2\pi$, where λ_{min} is the shortest wavelength of GWs in LIGO's frequency range. Variations in the GW in space can then be neglected, and only variations in time matter, leading to Eq. (3). However, if the interferometer is *larger* than wavelength of the GW, general relativity predicts that additional terms that depend on the velocity of the particle as well as the *spatial* variation of the GW—the magnetic part of the Weyl tensor of the GW—will now appear in Eq. (3). It is in principle possible to measure these new effects with MIGO; at 17 km, the length of the Space-based MIGO is comparable to the wavelength of a GW with a frequency of roughly 3 kHz. As can be seen in figure 7, there are a number of GW sources above this frequency that can potentially be used to probe these effects.

5 Conclusions

In the first part of this paper, we have explored the implications, broadly speaking, of non-Euclidean geometry for quantum physics. The problem of the interaction of gravitational radiation with quantum matter, including nonrelativistic quantum many-body-systems, was explored. In the second part of this paper, we have explored in detail one particular aspect of this problem, namely, the detection of astrophysical sources of the GWs by means of matter-wave interferometry (MIGO). Our theoretical analysis indicates that in terms of sensitivity, size, capability, and flexibility, the *quantum* methods embodied in MIGO have overwhelming advantages over the *classical* methods embodied in LIGO in studying general relativistic effects. What before took many kilometers can now be done in a couple hundred meters, and what took millions of kilometers can now be done with only thousands of meters. The impact of MIGO will go beyond simply being another astronomical instrument, however. With the advantage in MIGO that slowly moving atoms are predicted to have over ultrarelativistic ones, it will also spur theoretical and experimental studies that probe the intersection of *nonrelativistic* quantum mechanics with general relativity [17]. As an example,

we note that limitations to MIGO's sensitivity are, at their most fundamental level, imposed by quantum mechanics, and thus cannot be exceeded. Since MIGO in its essence measures local curvature, like Wigner [68, 69], we ask: What are the fundamental quantum limitations to the measurement of the Riemann curvature tensor arising from the uncertainty principle? This leads naturally to the age-old question, approached now from a different angle: What does it imply for Einstein's theory of general relativity, and for geometry as a whole, if curvature cannot be *measured* beyond these fundamental quantum limits? This question, which, in order to answer, was once thought to require energy scales on the order of the Planck energy—the energy where general relativity and the other forces of nature are expected unify—can now be addressed using matter-wave interferometry, once the fundamental quantum limits to MIGO's sensitivity have been established.

6 Acknowledgements:

ADS and RYC were supported by a grant from the Office of Naval Research. We thank Peter Bender, John Garrison, Theodore Hänsch, Jon Magne Leinaas, Andrew P. Mackenzie, Richard Marrus, Chris McKee, Joseph Orenstein, William D. Phillips, Marlan O. Scully, Jan Peter Toennies, and Rainer Weiss for many clarifying and insightful discussions.

A Brief Review of Gravitational Waves

In this appendix, we present a brief review of GWs in the linearized gravity limit; the reader is referred to [4] or [70] for a complete review.

Given a spacetime manifold $\mathcal{M}$, the metric $g_{\mu\nu}$ gives the measure of length, $ds^2 = g_{\mu\nu}dx^\mu dx^\nu$, on $\mathcal{M}$. The precise form of $g_{\mu\nu}$ depends on the coordinate system chosen, and if $\tilde{x}_\mu$ is another choice of coordinates, then the coordinates x_μ expressed in the coordinates $\tilde{x}_\mu$ is simply $x_\mu(\tilde{x})$. Since the length of a vector in $\mathcal{M}$ cannot depend on the choice of coordinate systems, $g_{\mu\nu}(x)dx^\mu dx^\nu = g_{\mu\nu}(\tilde{x})d\tilde{x}^\mu d\tilde{x}^\nu$, and by using the chain rule, we see that in a coordinate transformation the metric changes by

$$g_{\mu\nu}(\tilde{x}) = g_{\alpha\beta}(x)\frac{\partial x^\alpha}{\partial \tilde{x}^\mu}\frac{\partial x^\beta}{\partial \tilde{x}^\nu}. \tag{14}$$

No physically measurable quantities can depend on the choice of coordinates. In Newtonian gravity, and in special relativity, we require physics to be invariant under global coordinate transformations. In general relativity, we require the theory to be invariant under *general* coordinate transformations. Consequently, the choice of coordinate systems is often called a 'gauge choice', in analogy to EM, and general coordinate-transformation-invariance is often referred to as 'gauge invariance' [9].

We are interested in the propagation of GWs in the spacetime surrounding the Earth. Because of the relatively small mass of the Earth, the spacetime can be approximated as being flat. If $\eta_{\mu\nu} = diag(-1, 1, 1, 1)$ is the Minkowski metric, we can approximate $g_{\mu\nu} \approx \eta_{\mu\nu} + h_{\mu\nu}$, where the components of $h_{\mu\nu}$ are 'small' compared with unity, and $h_{\mu\nu}$ represents the 'strains' in the flat spacetime caused by the passage of a GW. It is treated as just another tensor on $\mathcal{M}$, and its indices are raised and lowered using $\eta_{\mu\nu}$: $h^\nu_\mu = \eta^{\nu\alpha}h_{\alpha\mu}$. In linearized gravity, we keep terms only linear in $h_{\mu\nu}$; since $g^{\mu\alpha}g_{\alpha\nu} = \delta^\mu_\nu$, $g^{\mu\nu} \approx \eta^{\mu\nu} - h^{\mu\nu}$.

Even though we are working in the linearized gravity limit, there is still a remnant of the coordinate transformation invariance Eq. (14) left. If $x_\mu = \tilde{x}_\mu + \xi_\mu$ where ξ_μ is a 'small', arbitrary vector, then from Eq. (14), $h_{\mu\nu}$ transforms to $\tilde{h}_{\mu\nu} = h_{\mu\nu} + \partial_\mu\xi_\nu + \partial_\nu\xi_\mu$. The similarity between the transformation of $h_{\mu\nu}$ under a *coordinate* transformation, and the transformation of the vector potential $A_\mu \to A_\mu + \partial_\mu\phi$ under a $U(1)$ *gauge* transformation is readily apparent. Being a symmetric, 2×2 tensor, $h_{\mu\nu}$ has ten components. We have the freedom, as with the vector potential in EM, to make specific choices for ξ_μ and its derivatives—eight variables in all—that will determine our coordinate system. Thus, $h_{\mu\nu}$ contains only $10 - 8 = 2$ physical degrees of freedom, or polarization states. The usual coordinate choice is the TT gauge: $\eta^{\mu\nu}h_{\mu\nu} = 0$, $\partial^\mu h_{\mu\nu} = 0$, and, for GWs in Minkowski space, the condition $h_{0\mu} = 0$ is automatically follows.

In the linearized gravity limit, the Levi-Civita connection is in general,

$$\Gamma^{\alpha}_{\mu\nu} = \frac{1}{2}\left(\partial_\mu h^\alpha_\nu + \partial_\nu h^\alpha_\mu - \partial^\alpha h_{\mu\nu}\right), \tag{15}$$

where $\partial_\mu \equiv \partial/\partial x^\mu$, while the Riemann curvature tensor and the Ricci tensor are, respectively

$$\begin{aligned} R^{\mu}{}_{\nu\alpha\beta} &= \frac{1}{2}\left\{\partial_\nu(\partial_\alpha h^\mu_\beta - \partial_\beta h^\mu_\alpha) + \partial^\mu(\partial_\beta h_{\nu\alpha} - \partial_\alpha h_{\nu\beta})\right\}, \\ R_{\mu\nu} &= -\frac{1}{2}\Box h_{\mu\nu} + \frac{1}{2}\partial_\mu\partial^\alpha h_{\alpha\nu} + \frac{1}{2}\partial_\nu\partial^\alpha h_{\alpha\mu} - \frac{1}{2}\partial_\mu\partial_\nu h^\alpha_\alpha, \end{aligned} \tag{16}$$

were $R_{\mu\nu} = R^\alpha_{\mu\alpha\mu}$. Consequently, $R \equiv \eta^{\mu\nu}R_{\mu\nu} = -\Box h^\mu_\mu + \partial_\mu\partial_\nu h^{\mu\nu}$. For GWs in the TT gauge, the above equations reduce even further, and we see that $R = 0$, $R_{0\mu} = 0$, and $R_{0i0j} = -\ddot{H}_{ij}/2$.

The evolution equation for GWs comes from Einstein's equation,

$$R_{\mu\nu} - \frac{1}{2}g_{\mu\nu}R = \frac{8\pi G}{c^4}T_{\mu\nu}, \tag{17}$$

where G is Newton's constant, and $T_{\mu\nu}$ is the energy-momentum tensor of matter in the spacetime. Away from all sources, $T_{\mu\nu} = 0$, and since $R = 0$, we find that $R_{\mu\nu} = 0$, or from Eq. (16), $\partial^\alpha\partial_\alpha h_{ij} = 0$, with the additional transversality condition $\partial^i h_{ij} = 0$. Thus, like an EM wave in the radiation gauge, h_{ij} in the TT gauge is a transverse wave that satisfies the wave equation. It also can be expanded in plane waves,

$$h_{ij} = \sum_{s=+,\times}\sum_{k_x k_y k_z} \epsilon^{(s)}_{ij}(k) h_s(k) e^{i(\vec{k}\cdot\vec{x}-\omega t)}, \tag{18}$$

were $\epsilon^{(s)}_{ij}(k)$ are the unit polarization vectors, and the transversality condition becomes $k^i\epsilon^{(s)}_{ij}(k) = 0$. Thus, in the plane perpendicular to $\vec{k}$, $\epsilon^{(s)}_{ij}$ can be represented by 2×2 matrices, where

$$\epsilon^{(+)} = \begin{pmatrix} 1 & 0 \\ 0 & -1 \end{pmatrix}, \qquad \epsilon^{(\times)} = \begin{pmatrix} 0 & 1 \\ 1 & 0 \end{pmatrix}.$$

Sketches of the force-field lines produced by these polarizations are drawn in figure 3.

B Calculation of MIGO Phase Shifts

We consider first the horizontal MIGO configuration figure 5. Assuming that the atoms in figure 5 are fast moving, in the absence of a GW the atoms travel along the straight-line paths as drawn. At time t_r, the rth atom is diffracted by the beam splitter, and for the $n = +1$ order, the path that the atom travels is: $v_{0y} = v_\perp$, $y_0(t) = v_\perp(t - t_r)$, and $v_{0x} = v_\parallel$, $x_0(t) = v_\parallel(t - t_r)$, for $t_r < t < t_r + T/2$, where $T/2$ is the time for the atom to travel from the beam splitter to the mirror. For $t_r + T/2 < t < t_r + T$ the path is: $v_{0y} = -v_\perp$, $y_0(t) = L_\perp - v_\perp(t - t_r)$, while $v_{0x} = v_\parallel$ and $x_0(t) = v_\parallel(t - t_r)$ still. Clearly, $L_\perp = v_\perp T$ and $L_\parallel = v_\parallel T$. The velocities $v_\perp$ and $v_\parallel$ are the initial velocities of the atom as it leaves the diffraction-grating beam splitter, and just like for light, $v_\perp = 2\pi\hbar/ma$ where a is the periodicity of the grating. Then $v_\parallel = (v_s^2 - v_\perp^2)^{1/2}$ where v_s is the velocity of the beam incident the beam splitter. Gravity can be neglected as long as $v_\parallel T >> gT^2/2$ where g is the acceleration due to Earth's gravity. Since our focus is on GWs, we approximate g as a constant, and neglect local curvature effects from stationary sources such as the Earth. A similar set of equations hold for the $n = -1$ order with $v_\perp \to -v_\perp$.

If a GW with $h_{ij}(t)$ is present, the paths of the atom will be slightly perturbed from straight lines, and we take $x = x_0 + x_1$ and $y = y_0 + y_1$, where x_1 and y_1 are deviations from the unperturbed paths x_0 and y_0. These perturbations satisfy the geodesic deviation equations of motion in Eq. (3), but with (x, y) approximated as (x_0, y_0) on the right hand side.

To take into account the action of the GW on the mirrors, we model the mirror and its connection to the frame of the interferometer as a spring with a resonance frequency f_0—which depends on the size of

the interferometer as well as its material properties—and a quality factor Q. We denote by $(X(t), Y(t))$ the position of the mirror along the $n = +1$ path, and since in the absence of a GW the mirror does not move, we take $X(t) = L_\parallel/2 + X_1(t)$, and $Y(t) = L_\perp/2 + Y_1(t)$, where $X_1(t)$ and $Y_1(t)$ are perturbations of the mirror's position due to the GW. They are also solutions of Eq. (3), but because the mirrors are connected to springs,

$$\frac{d^2X_1}{dt^2} + \frac{2\pi f_0}{Q}\frac{dX_1}{dt} + (2\pi f_0)^2 X_1(t) = \frac{1}{2}\frac{d^2h_{xx}}{dt^2}\left(\frac{L_\parallel}{2}\right) + \frac{1}{2}\frac{d^2h_{xy}}{dt^2}\left(\frac{L_\perp}{2}\right), \tag{19}$$

$$\frac{d^2Y_1}{dt^2} + \frac{2\pi f_0}{Q}\frac{dY_1}{dt} + (2\pi f_0)^2 Y_1(t) = \frac{1}{2}\frac{d^2h_{yy}}{dt^2}\left(\frac{L_\perp}{2}\right) + \frac{1}{2}\frac{d^2h_{xy}}{dt^2}\left(\frac{L_\parallel}{2}\right), \tag{20}$$

which are driven simple harmonic oscillators.

The action corresponding to the geodesic deviation equation is [71]

$$S = \int_{t_r}^{t_r+T} dt\left(\frac{1}{2}m\vec{v}^2 - \frac{1}{2}m\dot{h}_{ij}v^i x^j\right), \tag{21}$$

Writing $\vec{v} = \vec{v}_0 + \vec{v}_1$, we find that for the $n = +1$ path the change in the action due to the GW is

$$\begin{aligned}\frac{S_{+1}}{m} \approx L_\parallel\Bigg(&v_{1x}(t_r+T) - \frac{1}{2}L_\parallel\dot{h}_{xx}(t_r+T) + \frac{1}{2}v_\parallel h_{xx}(t_r+T) - \frac{1}{2}v_\perp\left[h_{xy}(t_r+T) - h_{xy}(t_r+T/2)\right]\Bigg) + \\ &\frac{L_\perp}{2}\left[v_{1y}(t_r+T^-/2) - v_{1y}(t_r+T^+/2)\right] + \frac{1}{2}v_\perp L_\perp h_{yy}(t_r+T/2) - \\ &\frac{1}{2}\int_{t_r}^{t_r+T}\left(v_\parallel^2 h_{xx}(t) + v_\perp^2 h_{yy}(t)\right)dt - v_\perp v_\parallel\left\{\int_{t_r}^{t_r+T/2} h_{xy}(t)\,dt - \int_{t_r+T/2}^{t_r+T} h_{xy}(t)\,dt\right\},\end{aligned} \tag{22}$$

after successive integration by parts of Eq. (21), and using Eq. (3). The velocities $v_{1y}(t_r + T^-/2)$ and $v_{1y}(t_r + T^+/2)$ are the perturbed velocities of the atom right before and right after the mirrors, respectively. Since the passage of the GW will shift the velocity of the mirrors as well as the atoms, a jump condition of the y-velocity at the mirror requires that

$$v_{1y}(t_r + T^+/2) = -v_{1y}(t_r + T^-/2) + V_{1y}(t_r + T/2). \tag{23}$$

Taking the Fourier transform of h_{ij}, and neglecting the transients in the solution of Eq, (20), we find for a horizontal MIGO that

$$\Delta\phi^{hor}_{MIGO}(f) = -\frac{m}{\hbar}\pi L_\perp L_\parallel i f h_\times(f) e^{-i\pi fT} F_h(fT), \tag{24}$$

for a GW with amplitude $h_\times(f)$ and frequency f. Only the $\times$ polarization causes a net phase shift in the interferometer; the + polarization does not, as can be seen due to the inherent bilateral symmetry of the interferometer. The horizontal resonance function is

$$F_h(fT) = 1 - 2e^{i\pi fT/2}\mathrm{sinc}\left(\frac{\pi fT}{2}\right) + \left[\mathrm{sinc}\left(\frac{\pi fT}{2}\right)\right]^2 - \frac{1}{2}\frac{f^2}{f^2 - f_0^2 + if_0 f/Q}, \tag{25}$$

where $\mathrm{sinc}(x) \equiv \sin x/x$. The analysis of the vertical configuration MIGO follows in the same way. The overall form of Eq. (24) still holds, with only the replacement $F_h(fT/4)$ by $2F_v(fT)$, where now

$$F_v(fT) = 1 - \left[\mathrm{sinc}\left(\frac{\pi fT}{2}\right)\right]^2 + \frac{i}{\pi fT/2}\left[1 - \mathrm{sinc}(\pi fT)\right] - \frac{1}{2}\frac{f^2}{f^2 - f_0^2 + if_0 f/Q}, \tag{26}$$

for this configuration.

If we consider the low frequency $f \to 0$ limit of Eqs. (25) and (26), we find that $F_h(fT) \approx -i\pi fT$, while $F_v \sim i\pi fT/3$, irrespective of how the mirror is mounted onto the frame of the interferometer. This is not the case in the high frequency limit. We find that in the infinitely-rigid interferometer limit where $f_0 \to \infty$, and then $f \to \infty$, both resonance factors approach one. If, however, the mirrors are freely suspended like those of LIGO, then $f_0 \to 0$ first. Then when the $f \to \infty$ limit is taken, both resonance functions approach one-half. In the MIGO graphs of figure 7, we took as the speed of sound for the material used to construct the interferometer frame as 6000 m/s, and that the motion of the mirrors were critically damped with $Q = 1$. This resulted in the small dips at the high-frequency end of the MIGO graphs.

C Effects of Thermal Noise on MIGO

We consider the mirrors to be rigidly attached to the frame of the interferometer. (This analysis can be repeated with the mirrors attached to springs as described in **Appendix B**). The finite temperature of the mirror induces fluctuations on the surface of the mirror, i. e., transverse surface sound waves, which will induce random Doppler-like shifts in the velocity of the atoms after it hits the mirror. Such velocity shifts are not important for LIGO because the speed of light is much larger compared to the velocity of these fluctuations. For slowly moving atoms, on the other hand, these fluctuations are important, and can potentially degrade the sensitivity of MIGO.

We model the surface of the mirror as a continuous sheet with transverse surface fluctuations $u(\vec{x},t) = u_0 \sin(\vec{k}_s \cdot \vec{x} - \omega_s t + \phi_s)$, where $\vec{x} = (x,y)$ is a vector at the surface of the mirror, $\vec{k}_s$ is the wavenumber of the sound mode, ω_s is its frequency, and ϕ_s is its random phase. The dispersion relation for the sound wave is $\omega_s = v_{sound} k_s$ where v_{sound} is the transverse speed of sound for the mirror. The surface of the mirror in the presence of the sound mode is defined by $z = u(\vec{x},t)$.

Consider an atom with wavefunction $\psi_{inc}(\vec{x},z,t) = A_0 \exp\{i(k_\perp z + \omega_\perp t)\}$ normally incident on the mirror. The reflected wavefunction $\psi_{ref}(\vec{x},z,t)$ is determined by the Schrödinger equation, and the boundary conditions that the total wavefunction vanishes at $z = u(\vec{x},t)$. The total current *normal to the surface of the mirror* vanishes there as well. Because this surface is changing with time, this is a moving boundary problem that cannot be solved exactly. We note, however, that for $\omega_s >> \omega_\perp$, the surface of the mirror oscillates many times during the time when the atom reflects off of it; these oscillations cancel each other, and do not adversely affect the motion of the atom. On the other hand, when $\omega_s << \omega_\perp$, the surface is frozen in time, and the problem reduces to an atom reflecting off a rough surface. It is straightforward to see that for this case any variations in the reflected atom's velocity normal to the mirror is due to changes in the direction of the normal vector to the surface of the mirror. This causes a velocity shift of the atom that is proportional to $(k_s u_0)^4$, and as we shall see, is not the dominant effect.

Consider now the case when $\omega_s \approx \omega_\perp$. Expanding ψ_{inc} at the surface of the mirror, we get

$$\begin{aligned} \psi_{ref}\left[\vec{x}, z = u(\vec{x},t), t\right] &= -A_0 \exp\{i\left(k_\perp u(\vec{x},t) + \omega_\perp t\right)\}, \\ &= -A_0 \sum_{q=-\infty}^{q=\infty} J_q(k_\perp u_0) \exp\left\{i\left(\omega_\perp - q\left[\vec{k}_\perp \cdot \vec{x} - \omega_s t + \phi_s\right]\right)\right\}. \end{aligned} \tag{27}$$

The mirror surface acts as a FM modulator, and produces sidebands with an initial amplitude given by the qth order Bessel function $J_q(k_\perp u_0)$. The amplitude of the mode $u_0 = v_{th}/\omega_s$, where $v_{th} = (k_B T_{mirr}/M)^{1/2}$ with T_{mirr} the temperature of the mirror with mass M, while $k_\perp = 2\pi/a$, where a is the periodicity of the diffraction grating used in the beam splitter. The product $k_\perp u_0 = k_\perp v_{th}/\omega_s \approx k_\perp v_{th}/\omega_\perp = v_{th}/v_\perp << 1$. Consequently, only the $q = 1$ sideband is important (since $\omega_\perp \approx \omega_s$, the $q = -1$ sideband is not a propagating mode).

Thus, since $J_0(k_\perp u_0) \approx 1$, the incident wavefunction is reflected backward with almost the same amplitude it came in with, but now an additional $q = 1$ component with amplitude $J_1(k_\perp u_0)$ mixed in. But because the phase of the sound mode is arbitrary, the wavenumber of this reflected wave is approximately $-k_\perp + k_1 (v_{th}/v_\perp)^2/2$, where $k_1 = (4m\omega_\perp/\hbar)^{1/2}$ is the wavenumber of the $q = 1$ reflected wavefunction. The linear term in the expansion of $J_1(k_\perp u_0)$ vanishes since roughly half the time the sound mode is in phase with the incident atom, and half the time it is out of phase. Thus, the fractional change in the atom's velocity is due to thermal motion of the mirror is $\Delta v/v_\perp = (v_{th}/v_\perp)^2$, and is independent of the material properties of the mirror, as expected. This shift in the atom's velocity introduces a thermal-noise-limited sensitivity

$$\tilde{h}(f)_{th} = \frac{L_\perp \Delta v}{2\pi A |F(fT)| f^{3/2}}, \tag{28}$$

which dies out faster than the shot-noise-limited sensitivity $\tilde{h}(f)_{shot} \sim 1/f$ for high frequencies, but it is dominant for low frequencies. The thermal- and shot-noise-limited sensitivities are equal at $f_{turn} = \dot{N}(mL_\perp \Delta v/\hbar)^2$. For a one-kilogram-mass mirror at a temperature of 1 K with a 6000 m/s transverse speed of sound, this is roughly $10^{-7} - 10^{-8}$ Hz for the ^{133}Cs atom MIGOs shown in figure 7, and causes the curves

of the Earth-based vertical MIGO and the Space-based MIGO to angle slightly upwards at low frequencies. For the Earth-based horizontal MIGO this frequency is roughly 10^{-12}, and thermal effects are negligible.

References

[1] Spivak, M., 1979, A Comprehensive Introduction to Differential Geometry, Vol. I, 2nd edition (Publish or Perish: Berkeley).

[2] Spivak, M., 1979, A Comprehensive Introduction to Differential Geometry, Vol. II, 2nd edition (Publish or Perish: Berkeley).

[3] Landau, L. D. and Lifshitz, E. M., 1965, The Classical Theory of Fields, 2nd Edition (Pergamon: London), p. 301.

[4] Misner, C. W., Thorne, K. S., and Wheeler, J. A., 1973, Gravitation (W. H. Freeman and Company: San Francisco), Chapters 1, 35.

[5] Pound, R. V., and Rebka, G. A., 1960, Physical Review Letters, 4, pp. 337-341.

[6] Collela, R., Overhauser, A. W., and Werner, S. A., 1975, Physical Review Letters, 34, pp. 1472-1474.

[7] Thorne, K. S., 1997, 300 Years of Gravitation, edited by S. W. Hawking and W. Isreal, (Cambridge University Press: New York) pp. 330-458.

[8] This analogy is usually made between GWs and non-Abelian field theories such as $SU(2)$ [9]. We will, bowever, be working in the linearized gravity limit where the non-linear aspects of GWs are neglected. In this limit, the analogy with EM holds well.

[9] Yang, C. N., 1983, Selected Papers 1945-80 with Commentary, (W. H. Freedman and Company: San Francisco), pp. 73-74.

[10] Synge, J. L., 1960, Relativity: The General Theory, (North-Holland Publishing Co.: Amsterdam), Chapter 2.

[11] de Felice, F. and Clarke, C. J. S., 1990, Relativity on Curved Manifolds, (Cambridge University Press: Cambridge), Chapter 9.

[12] Speliotopoulos, A. D. and Chiao, R. Y., Coupling of linearized gravity to non-relativistic test particles: Dynamics in the general laboratory frame. To be published in Physical Review D, gr-qc/0302045.

[13] Local coordinate systems fixed to an observer have been constructed before. The Fermi-Normal coordinates were constructed in the 1920's by Fermi [14], and the Fermi-Walker coordinates were constructed in [10]. Because of a number of assumptions made in their construction, they are not that useful in dealing with arbitrary GWs.

[14] Fermi, E., 1922, Atti della Academia Nazionale Lincei Rendus Class di Scienze Fisiche Matematiche e Naturali, 31, pp. 21-24, 51-52.

[15] Berry, M. V., 1984, Proceedings of the Royal Society of London, A392, pp. 45-57; Cai, Y. Q. and Papini, G., 1990, Classical and Quantum Gravity, 7, pp. 269-275; Cai, Y. Q. and Papini, G., 1990, General Relativity and Gravitation, 22, pp. 259-267.

[16] Chiao, R. Y., 1982, Physical Review, B25, pp. 1655-1662.

[17] Chiao, R. Y., 2004, gr-qc/0303100, Science and Ultimate Reality: Quantum Theory, Cosmology and Complexity, edited by J. D. Barrow, P. C. W. Davies, and C. L. Harper Jr., (Cambridge University Press: Cambridge), Chapter 13.

[18] Weinberg showed in [19] that when one attempts to generate a GW by means of an acoustical excitation of a Weber bar, the majority of the energy in the bar is dissipated as heat. Only a small fraction of this energy is converted into GWs. While valid for classical systems like the Weber bar, this analysis often fails for quantum many body systems such as the quantum Hall fluid, where the existence of a finite energy gap allows for macroscopic, dissipationless quantum flows in the fluid.

[19] Weinberg, S., 1972, Gravitation and Cosmology: Principles and Applications of the General Theory of Relativity (John Wiley and Sons: New York).

[20] Chiao, R. Y. and Fitelson W. J. , 2003, Time and matter in the interaction between gravity and quantum fluids: Are there macroscopic quantum transducers between gravitational and electromagnetic waves?, gr-qc/0303089. Chiao, R. Y., Fitelson, W. J. and Speliotopoulos, A. D., 2003, Search for quantum transducers between electromagnetic and gravitational radiation: A measurement of an upper limit on the transducer conversion efficiency of yttrium barium copper oxide, gr-qc/0304026.

[21] Mackenzie, A. P. and Maeno, Y., 2003, Review of Modern Physics, 75, pp. 657-713.

[22] Aoki, D, Huxley, A., Ressourche, E., Braithwaite, D., Flouguet, J., Brison, J.-P., Lhotel, E., and Paulsen, C., 2001, Nature, 413, pp. 613-616.

[23] Scully, M. O. and Dowling, J. P., 1993, Physical Review, A48, pp. 3186-3190.

[24] Budker, D., Kimball, D. F., and DeMille, D. P., 2003, Atomic Physics: An Approach through Problems (Oxford University Press: New York) p. 301.

[25] Gustavson, T. L., Bouyer, P., and Kasevich, M. A., 1997, Physical Review Letters, 78, pp. 2046-2049.

[26] Gustavson, T. L., Landragin, A., and Kasevich, M. A., 2000, Classical and Quantum Gravity, 17, pp. 2385-2398.

[27] Keith, D. E., Ekstrom, C. R., Turchette, Q. A., and Pritchard, D. E., 1991, Physical Review Letters, 66, pp. 2693-2396; Riehle, F., Kisters, T., Witte, A., Helmcke, J., and Bordé, C., 1991, Physical Review Letters, 67, pp. 177-180; reference [46].

[28] Linet, B., and Tourrenc, Ph., 1976, Canadian Journal of Physics, 54, pp. 1129-1133.

[29] Stodolsky, L. 1979, General Relativity and Gravitation, 11, pp. 391-405.

[30] Anandan, J., 1977, Physical Review, D15, pp. 1448-1457.

[31] Anandan, J., 1981, Physical Review, D24, pp. 338-346.

[32] Anandan, J., 1996, Physical Review, 53, pp. 779-786.

[33] Anandan, J. and Chiao, R. ,Y., 1982, General Relativity and Gravitation, 14, pp. 515-521.

[34] Cai, Y. Q., and Papini, G., 1989, Classical and Quantum Gravity, 6, pp. 407-418.

[35] Bordé, C. J., 1997, Atom Interferometry, edited by P. R. Berman, (Academic Press: San Diego) pp. 257-292.

[36] Bordé, C. J., Karasiewicz, A., and Tourrenc, Ph., 1994, International Journal of Modern Physics, D3, pp. 157-161.

[37] Bordé, C. J., 2001, Comptes Rendus, 2, pp. 509-530.

[38] In preparation.

[39] While the sensitivity of LIGO can be, in principle, improved using squeezed light [40], the sensitivity of MIGO can be, in principle, improved by using squeezed atom states as well [41]. While the practicality of using squeezed light is still in question, squeezed fermionic number states are very robust.

[40] Caves, C. M., Thorne, K. S., Drever, R. W. P., Sandberg, V. D., and Zimmermann, M., 1980, Review of Modern Physics, 52, pp. 341-392.

[41] Goldstein, E. V., Moore, M. G., and Meystre, P., 2000, Laser Physics, 10, pp. 8-14.

[42] Chiao, R. Y. and Speliotopoulos, A. D., 2003, International Journal of Modern Physics, D12, pp. 1627-1632.

[43] Berman, P. R., editor, 1997, Atom Interferometry, (Academic Press: San Diego).

[44] Peters, A. , Chung, K. Y., and Chu, S., 2001, Metrologia, 38, pp. 25-61.

[45] Scoles, G., editor, 1992, Atomic and Molecular Beam Methods, Vols. 1, 2, (Oxford University Press: New York).

[46] Kasevich M. A. and Chu, S., 1991, Physical Review Letters, 67, pp. 181-184.

[47] Packard, R. E., 1998, Review of Modern Physics, 70, pp. 641-651.

[48] Davis, J. C. and Packard, R. E., 2002, Review of Modern Physics, 74, pp. 741-773.

[49] Arndt, M., Nairz, O., Voss-Andreae, J., Keller, C., Van der Zouw, G., and Zeilinger, A., 1999, Nature, 401, pp. 680-682.

[50] Private communication with J. P. Toennies, Max Planck Institut für Strömungsforschung, 37073 Göttingen, Germany.

[51] Bradley, C. C. and Hulet, R., 1996, Atomic, Molecular, and Optical Physics: Atoms and Molecules, edited by F. B. Dunning, and R. G. Hulet, (Academic Press: New York) pp. 129-144.

[52] Powers, D. E., Hansen, S. G., Guesic, M. E., Puiu, A. C., Hopkins, J. B., Dietz, T. G., Duncan, M. A., Lanridge-Smith, P. R. R., and Smalley, R. E., 1982, Journal of Physical Chemistry, 86, pp. 2556-2560.

[53] Willmott P. R. and Huber, J. R., 2000, Review of Modern Physics, 72, pp. 315-328.

[54] Robertson, N. A., 2000, Classical and Quantum Gravity, 17, pp. R19-R40.

[55] B. C. Barish, 2002, LIGO overview, NSF annual review 23-Oct-02, http://www.ligo.caltech.edu/LIGO_web/conferences/nsf_reviews.html.

[56] B. C. Barish, 1999, 1999 Meeting of the Division of Particles and Fields of the American Physical Society, edited by K. Arisaka and Z. Bern. Published electronically by the University of California, Los Angeles, http://www.dpf99.library.ucla.edu/browsedpf99.html.

[57] Tyson, J. T. and Giffard, R. P., 1978, Annual Review of Astronomy and Astrophysics, edited by G. Burbidge, D. Layzer, and J. G. Phillips (Annual Reviews, Inc.: Palo Alto) pp. 521-554.

[58] Stodolsky briefly mentioned the use of the synchronous coordinates as a justification for not considering the action of GWs with parts of the interferometer. This approach is in conflict with the usual coordinate system chosen to detect GWs.

[59] Buckland, J. R., Holst B. and Allison, W., 1999, Chemical Physics Letters, 303, pp. 107-110; Carnal, O. and Mlynek, J., 1991, Physical Review Letters, 66, pp. 2689-2692.

[60] By which we mean that $v_{sound}/L_{charac} >> f$, where L_{charac} is the characteristic length of the interferometer, and v_{sound} is the speed of the sound of the material used to construct it.

[61] Kasevich, M. A., Riss, E., and Chu, S., 1989, Physical Review Letters, 63, pp. 612-616.

[62] Fritschel P., 2003, Proceedings of SPIE, Gravitational Wave Detection, Vol. 4856, edited by M. Cruise, and P. Saulson, (SPIE: Bellingham).

[63] Cutler, C. and Thorne, K. S., 2002, Proceedings of the 16th International Conference on General Relativity and Gravitation, edited by N. T. Bishop and S. D. Maharaj, (World Scientific: Singapore) pp 72-111.

[64] www.elec.gla.ac.uk/groups/nano/litho/32nmgrating.html.

[65] Buchenau, H., Knuth, E. L., Northby, J., Toennies, J. P., and Winkler, C., 1990, Journal of Chemical Physics, 92, pp. 6875-6889.

[66] Butt, N. M., Bashir, J., Willis, B. T. M., and Heger, G.. 1988, Acta Crystallogia, A44, pp. 396-398 (1988).

[67] Weare, J. H., 1974, Journal of Chemical Physics, 61, pp. 2900-2910.

[68] Wigner, E. P., 1957, Review of Modern Physics, 29, pp. 255-268.

[69] Salecker H. and Wigner, E. P., 1958, Physical Review, 109, pp. 571-577.

[70] Wald, R., 1984, General Relativity, (The University of Chicago Press: Chicago), Chapter 3.

[71] Speliotopoulos, A. D., 1995, Physical Review, D51, pp. 1701-1709.

[72] Blair, D. L. , 1991, The Detection of Gravitational Waves, ed. by D. L. Blair, (Cambridge University Press: Cambridge), p. 14.

[73] Hughes, S. and Thorne, K. S., 1998, Physical Review, D58, 122002.